GL-TR-89-0276

Polar Code Validation

I. Katz
J. R. Lilley, Jr.
G. A. Jongeward
M. J. Mandell
T. T. Luu

S-CUBED,
A Division of Maxwell Laboratories, Inc.
P.O. Box 1620
La Jolla, California 92038-1620

September 30, 1989

Final Report
Period Covering May 6, 1986 through September 6, 1989

Geophysics Laboratory
Air Force Systems Command
United States Air Force
Hanscom Air Force Base, MA 01731

" This technical report has been reviewed and is approved for publication "

DAVID L. COOKE
Contract Manager

CHARLES P. PIKE
Branch Chief

FOR THE COMMANDER

RITA C. SAGALYN
Division Director

This report has been reviewed by the ESD Public Affairs Office (PA) and is releasable to the National Technical Information Service (NTIS).

Qualified requestors may obtain additional copies from the Defense Technical Information Center. All others should apply to the National Technical Information Services.

If your address has changed, or if you wish to be removed from the mailing list, or if the addressee is no longer employed by your organization, please notify AFGL/DAA, Hanscom AFB, MA 01731. This will assist us in maintaining a current mailing list.

Do not return copies of this report unless contractual obligations or notices on a specific document requires that it be returned.

REPORT DOCUMENTATION PAGE

1a REPORT SECURITY CLASSIFICATION Unclassified	1b RESTRICTIVE MARKINGS
2a SECURITY CLASSIFICATION AUTHORITY N/A	3 DISTRIBUTION/AVAILABILITY OF REPORT Approved for public release; distribution unlimited
2b DECLASSIFICATION/DOWNGRADING SCHEDULE N/A	
4 PERFORMING ORGANIZATION REPORT NUMBER(S) SSS-DFR-89-10708/R1	5 MONITORING ORGANIZATION REPORT NUMBER(S) GL-TR-89-0276
6a NAME OF PERFORMING ORGANIZATION S-CUBED Division of Maxwell Laboratories, Inc.	6b OFFICE SYMBOL (If applicable)
7a NAME OF MONITORING ORGANIZATION Geophysics Laboratory	
6c ADDRESS (City, State, and ZIP Code) P. O. Box 1620 La Jolla, CA 92038-1620	7b ADDRESS (City, State, and ZIP Code) Hanscom AFB Massachusetts 01731-5000
8a NAME OF FUNDING/SPONSORING ORGANIZATION Geophysics Laboratory	8b OFFICE SYMBOL (If applicable)
9 PROCUREMENT INSTRUMENT IDENTIFICATION NUMBER F19628-86-C-0056	
8c ADDRESS (City, State, and ZIP Code) Hanscom AFB Massachusetts 01731-5000	10 SOURCE OF FUNDING NUMBERS

PROGRAM ELEMENT NO	PROJECT NO.	TASK NO.	WORK UNIT ACCESSION NO.
62101F	7601	30	AA

11 TITLE (Include Security Classification)
POLAR Code Validation

12 PERSONAL AUTHOR(S)
I. Katz, J. R. Lilley, Jr., G. A. Jongeward, M. J. Mandell, T. T. Luu

13a TYPE OF REPORT	13b TIME COVERED	14 DATE OF REPORT (Year, Month, Day)	15 PAGE COUNT
Final Report	FROM 5/1986 TO 9/1989	1989 September 30	58

16 SUPPLEMENTARY NOTATION

17 COSATI CODES			18 SUBJECT TERMS (Continue on reverse if necessary and identify by block number)
FIELD	GROUP	SUB-GROUP	Spacecraft Charging; POLAR Code; Auroral Charging; SPEAR I; Plasma Sheaths; CHARGE II

19 ABSTRACT (Continue on reverse if necessary and identify by block number)

The POLAR code was written to model charging by large spacecraft in low, polar orbit. This report documents comparisons of POLAR code calculations with flight experiments. Calculations of the plasma wake behind the Shuttle Orbiter are compared with the situ measurements of Murphy et al. [1989]. Calculations of the charging of DMSP-7, performed by Dr. David Cooke for the GL, are compared with the flight measurements of Gussenhoven et al. [1985]. Calculations of current and potential on the SPEAR I rocket are compared with the flight measurements. Calculation of electron collection by the CHARGE II mother rocket payload are compared with the flight observations of Myers et al. [1989]. In all cases, the POLAR calculations agreed with the essential features of the observations.

20 DISTRIBUTION/AVAILABILITY OF ABSTRACT	21 ABSTRACT SECURITY CLASSIFICATION	
☐ UNCLASSIFIED/UNLIMITED ☐ SAME AS RPT ☐ DTIC USERS	Unclassified	
22a NAME OF RESPONSIBLE INDIVIDUAL Dr. David L Cooke	22b TELEPHONE (Include Area Code) (617) 377-2931	22c OFFICE SYMBOL GL/PHK

TABLE OF CONTENTS

1. INTRODUCTION

> *"A workshop on Natural Charging of Large Space Structures in Near Earth Polar Orbits, sponsored by the Air Force Geophysics Laboratory and Boston College, was held on 14 and 15 September, 1982, at AFGL. Many of the specialists in the area of spacecraft charging problems assembled to discuss the necessity and/or possibility of developing realistic, effective codes describing the interaction of low-earth orbiting systems with the environment. ...There are considerable differences of opinion among specialists in this area concerning the nature and magnitude of the problems and the feasibility of developing realistic models or codes to deal with them."* [1]

The POLAR code was started amidst controversy. At the workshop, questions were raised about whether large objects would charge in polar orbit and whether it was possible to model the relevant physics. Others expressed concerns about how resultant computer models could be validated. The polar orbit charging question was answered and observed by Geophysics Laboratory (GL) instruments mounted on DMSP spacecraft.

The POLAR code was written to model charging by large spacecraft in low, polar orbit. This report documents comparisons of POLAR code calculations with flight experiments. Calculations of the plasma wake behind the Shuttle Orbiter are compared with in the situ measurements of Murphy et al. [1989]. Calculations of the charging of DMSP-7, performed by Dr. David Cooke of the GL, are compared with the flight measurements of Gussenhoven et al. [1985]. Calculations of current and potential on the SPEAR I rocket are compared with the flight measurements. Calculation of electron collection by the CHARGE II mother rocket payload are compared with the flight observations of Myers et al. [1989]. In all cases, the POLAR calculations agreed with the essential features of the observations.

The Shuttle Orbiter and SPEAR I comparisons were intended to be with preflight predictions. In both cases, however, malfunctions during the flights

[1] Proceedings of the Air Force Geophysics Laboratory Workshop on Natural Charging of Large Space Structures in Near Earth Polar Orbit: 14-15 September 1982.

changed important parameters and required new calculations. The Orbiter main engine shut down early, lowering the orbit by a hundred kilometers. A cap on the SPEAR I plasma contactor didn't open allowing potentials of thousands of volts to appear on the rocket chassis. In both cases, the POLAR calculations were redone using the same model used for the preflight calculations, but with parameters appropriate for the actual flight.

This validation document has three parts in addition to the introduction: the first is a summary of the physics learned during the POLAR development and validation; the second is a discussion of the physical processes modeled by the POLAR code; the third part is a collection of papers that discuss the comparisons with the flight data.

2. SUMMARY OF POLAR ACHIEVEMENTS

> *"In brief, we require of new theories that they account for the results predicted by existing theories and that, in addition, they predict new results."* [2]

The POLAR development and validation efforts have lead to predictions and a new level of understanding about the physical mechanisms that determine spacecraft plasma interactions with the ionosphere. POLAR has answered many long, outstanding questions. The details are contained in the attached papers, and the validity of the results is born out by direct comparison with observations. The following paragraphs summarize POLAR's most significant contributions to spacecraft interaction physics. In each case, the results would not have been possible without the data and cooperation of the flight experimenters.

1. The physical processes controlling the plasma wake of large (~10 meter) spacecraft have been elucidated and compared with observation.

   Ions are accelerated into the plasma void behind large satellites by density gradient electric fields. The POLAR comparison with in situ measurements of the orbiter wake [Murphy & Katz, 1989] showed that the density over shoots and wake structure seen in laboratory experiments were not relevant to spacecraft in the ionosphere.

   √ POLAR includes the physics necessary to model wakes.

2 Auroral charging is predictable and increases with spacecraft size.

   POLAR was developed to pursue the speculations of Parks & Katz [1981]. POLAR was just one part of a Geophysics Laboratory (GL) investigation into auroral charging. Measurements of auroral charging on DMSP were reported by Gussenhoven et al. [1985] on DMSP. POLAR calculations by

[2] M.S. Gussenhoven, Proceedings of the Air Force Geophysics Laboratory Workshop on Natural Charging of Large Space Structures in Near Earth Polar Orbit: 14-15 September 1982, Chapter 31, "Requirements for Validating System Models".

Cooke et al. [1989] using data provided by Gussenhoven, reproduced the observed levels of charging. The POLAR calculations also showed that a small satellite would have charged to just a few volts.

√ POLAR includes the physics necessary to model auroral charging.

3. Electron collection from the ionosphere by active experiments is magnetically limited except at low (<250 km) altitudes.

POLAR calculations of the CHARGE II mother payload showed that the data of Meyers et al. [1989] actually agreed with magnetic limiting, contrary to much speculation in the literature. The POLAR model of the rocket had the correct finite cylinder geometry, and collected current in agreement with the measurements. The POLAR currents were substantially larger than the spherical probe results previously applied to the problem. The SPEAR I calculations [Katz et. al., 1989] showed how deviations from spherical symmetry enable electrons to cross magnetic field lines and be collected by high-voltage probes. In neither case was any "turbulence" necessary to explain the experimental results.

√ POLAR includes the physics necessary to model plasma sheaths.

3. POLAR CODE PHYSICAL MODELS

Below are outlined the basic physics models solved in POLAR. More details on the algorithms used to implement the models are contained in the *POLAR Code Users Manuals*.

3.1 PLASMA SHEATH

POLAR solves Poisson's equation in the volume surrounding a spacecraft.

$$\nabla^2\phi = \frac{\rho}{\varepsilon_0} \tag{1}$$

For potentials, ϕ, small compared with the background plasma temperature θ, the space-charge density, ρ, is calculated assuming linear screening:

$$-\frac{\rho}{\varepsilon_0} = \frac{\phi}{\lambda^2} \quad , |\phi| \le \phi_{sheath} \tag{2}$$

where $\phi_{sheath} \cong \theta \ln 2$, (3)

the potential where linear shielding breaks down [Parrot, Storey, Laframboise & Parker, 1982]. In many cases, the value used in POLAR for ϕ_{sheath} is higher, due to numerical accuracy considerations, but even for the most extreme cases, it is less than a few volts. This value sets the the low potential accuracy limit of the code.

For larger potentials, the space charge density is calculated by tracking representative macro particles in a fixed potential,

$$\ddot{\mathbf{x}} = \frac{q}{m}(\dot{\mathbf{x}} \times \mathbf{B} - \nabla\phi) . \tag{4}$$

The potentials are assumed to remain steady during a particle transit through the sheath. This sets the lower bound on the timescales, which can be modeled using POLAR. Potentials and charge densities are iterated until a self-

consistent solution is obtained. To speed convergence, an analytical estimate of the space-charge density is used to obtain the initial potential iterate.

3.2 NATURAL CHARGING

Surface potential, ϕ, changes are calculated using the capacitance, C, between the surface and the underlying chassis ground,

$$C\frac{d\phi}{dt} = j_{net} \times A, \tag{5}$$

where A is the surface area. The net current density has several components,

$$j_{net} = j_e^{incident} \times \left(1 - Y_e^{secondary\ e} - B_e^{backscatter\ e}\right) + j_{ion}^{sheath} \times \left(1 + Y_{ion}^{secondary\ e}\right) - j_e^{photo} \tag{6}$$

The incident ion currents are calculated by tracking particles through the sheath. The incident electron current has both a low and high energy component. The low energy component is treated as a single temperature Maxwellian and accurately represents the cold, dense ionospheric background. The high energy component is used to represent auroral electron fluxes and can be of the form

$$j(E) = aE(E - e\phi)^{-(\alpha+1)} + n\sqrt{\frac{kT}{2\pi m}}\left(\frac{1}{\pi(kT)^2}\right)Ee^{-(E-e\phi)/kT} + bEe^{-(E-E_0)^2/\delta^2} \tag{7}.$$

This form has been shown to fit inverted-V spectra [Fontheim et al.,1982].

3.3 PLASMA WAKE

The model of the wake structure used by POLAR depends on the position relative to the so-called ion front. This ion front marks the boundary where electron density begins to change on a scale commensurate with the Debye length and the ion density takes a sudden and dramatic drop. Ahead of the ion front, the plasma is treated as rarefied; its motion is controlled by the thermal spread in ion velocities. Behind the front, the motion is controlled by the electron temperature and ion mass.

The governing equations in this region ahead of the front, considering that electrons are more mobile than ions and that they maintain equilibrium with a local potential, are:

the Boltzman relation; $$n_e = n_o \exp(e\phi/kT_e) \tag{8}$$

continuity; $$\frac{\partial n_i}{\partial t} + \frac{\partial}{\partial z}(n_i v) = 0 \tag{9}$$

equation of motion; $$\frac{\partial v}{\partial t} + \frac{v\partial v}{\partial z} = \frac{-e}{M}\frac{\partial \phi}{\partial z} \tag{10}$$

Poisson's equation; $$\frac{\partial^2 \phi}{\partial z^2} = 4\pi e(n_e - n) \tag{11}$$

where
- n_o = ambient density
- n_i = ion density
- n_e = electron density
- θ_e = electron temperature
- e = electron charge
- ϕ = local potential
- k = Boltzman's constant

z is a variable representing distance parallel to the front velocity or, in the case of POLAR, perpendicular to the orbital velocity.

Crow et al. [1975] have numerically solved the above equations to predict the position of the ion front. POLAR uses an analytical fit to the Crow results [Katz et al., 1985]:

$$z_F(t) = 2\lambda_d \left\{ \left(\omega t + \frac{1}{\alpha}\right) \ln(1+\alpha\omega t) - \omega t - \left(1 - \frac{.429}{\alpha}\right)\left(\omega t - \frac{1}{\alpha}\ln(1+\alpha\omega t)\right) \right\}$$

$$\text{where } \omega = \frac{(4\pi n_o e^2)^{\frac{1}{2}}}{M}, \quad \lambda_d = \frac{(k\theta_e)^{\frac{1}{2}}}{4\pi n_o e^2} \tag{12}$$

are the ion plasma frequency and Debye length. α is a free parameter determined to be ~ 1.6.

Katz et al. [1985] showed that this formula agrees well with laboratory data from Wright et al. [1985]. Ahead of this front z_F, the plasma is assumed to expand due to thermal motion, the so-called "neutral approximation". Behind z_F the plasma evolves into a state that is self-similar [Chan et al., 1984]. The self-similar solution of equations 8-11 for $z > S_o t$ is

$$n = n_o \exp\left\{-\left(\frac{z + S_o t}{S_o t}\right)\right\} \tag{13}$$

where $S_o = (k\theta_e/M)^{\frac{1}{2}}$ is the ion acoustic speed.

We take the time variable to be spatially defined as:

$$t = \frac{x}{V_o} \tag{14}$$

where x is the distance behind the object (perpendicular to z) and V_o is the orbital velocity.

The wake routines in POLAR employ both limiting cases: (1) ahead of the ion front the electric field is negligible and the motion of ions is identical to neutrals; (2) behind the ion front, whose position is determined by equation (12), the quasi-neutral, self-similar solution of equation (13) is implemented.

POLAR has routines that accurately model the geometry of the object, and the "neutral ion" trajectories are calculated from:

$$f_i(\vec{x},v) = g(\vec{x},\Omega)\, f_{io}(\vec{v}) \tag{15}$$

where $f_{io}(\vec{v})$ is the unperturbed distribution function for a drifting Maxwellian; $g(\vec{x},\Omega)$ has value "0" if a ray starting from $\vec{x}$ and going in the direction Ω would strike the vehicle, and "1" if it would not.

The local density is given by:

$$n_i = (\vec{x}) \int f_i(\vec{x},\vec{v}) = \int g(\vec{x},\Omega) \left\{ \int f_{io}(\vec{v},\Omega)\, v^2 dv \right\} d\Omega \qquad (16)$$

This initial density calculated in three dimensions for neutral particles is compared with density calculated assuming the complex geometric object is replaced by a flat plate at a position where the dominant source appears at the object edge. This ratio provides a "geometric correction factor" that is applied to the quasi-neutral, one-dimensional solution discussed above for positions behind z_F. In this way, POLAR can calculate quite rapidly an approximate value for the ion and electron densities in the wakes of complex objects.

Note that the assumptions behind the front are: (1) the electron temperature and ion mass govern the equation of motion; (2) the plasma is quasi-neutral; (3) the magnetic field does not affect the ion or electron motion; (4) equation (12) serves as a good approximation for determining the boundary of the ion front; and (5) the geometric correction factor calculated in detail with the 3–dimensional neutral model can be approximately applied to correct the plasma densities as well. Therefore, the algorithm can address complex geometries but takes advantage of the smooth wake structure characteristic of ionospheric plasmas where $\theta_i/\theta_e \approx 1$.

4. FLIGHT DATA COMPARISON PAPERS

The papers on the following pages discuss POLAR code model comparisons with flight data.

JOURNAL OF GEOPHYSICAL RESEARCH, VOL. 94, NO. A2, PAGES 1450–1458, FEBRUARY 1, 1989

Structure of the Bipolar Plasma Sheath Generated by SPEAR I

I. KATZ,[1] G. A. JONGEWARD,[1] V. A. DAVIS,[1] M. J. MANDELL,[1] R. A. KUHARSKI,[1] J. R. LILLEY, JR.,[1] W. J. RAITT,[2] D. L. COOKE,[3] R. B. TORBERT,[4] G. LARSON,[4] AND D. RAU[4]

The Space Power Experiment Aboard Rockets I (SPEAR I) biased two 10-cm radius spheres as high as 46,000 V positive with respect to an aluminum rocket body. The experiment measured the steady state current to the spheres and the floating potential of the rocket body. Three-dimensional calculations performed using NASCAP LEO and POLAR 2.0 show that both ion-collecting and electron-collecting sheaths were formed. The rocket body potential with respect to the ionospheric plasma adjusted to achieve a balance between the electron current collected by the spheres and the secondary electron-enhanced ion current to the rocket body. This current balance was obtained with a large ion-collecting sheath that enveloped most of the electron-collecting sheath and reduced the area for collection of ionospheric electrons. The calculated current is in agreement with the flight measurement of a steady state current of less than 1.10 A. The calculations show that the rocket body was driven thousands of volts negative with respect to the ionospheric plasma. The calculated rocket potential is within the uncertainty of that inferred from ion spectrometer data. The current flowed through the space plasma. There was almost no direct charge transport between the spheres and the rocket body.

INTRODUCTION

Since the first time that electron guns were placed on rockets, the voltage on a rocket necessary to collect ionospheric electrons and complete the circuit has been the subject of much debate [*Winckler*, 1980]. Classical theories [*Langmuir and Blodgett*, 1924; *Mott-Smith and Langmuir*, 1926; *Beard and Johnson*, 1961; *Chen*, 1965; *Laframboise and Rubinstein*, 1976; *Rubinstein and Laframboise* 1978, 1982, 1983; *Parker and Murphy*, 1967] predict that even for low-current electron beams (less than 100 mA), rocket bodies will charge to thousands of volts. Early experiments, however, measured potentials of less than 100 V for beam currents as high as an ampere (see *Winkler* [1980] for a review of the experiments). Theoreticians questioned the validity of the measurements; experiments dismissed the theories as obviously irrelevant. In more recent years, experiments performed above 300 km produced measurements more in agreement with theoretical predictions [*Maehlum et al.*, 1988]. Using tethered subsatellites (so-called "mother-daughter" payloads), potentials have been measured more reliably. While at low altitudes the measured rocket potentials remain low, the results for higher-altitude rockets tend to agree with classical theories of space-charge limited collection. The low-altitude results are thought to stem from ionization of neutral gas within the electron collecting sheath [*Lai et al.*, 1985]. Still unresolved, owing to the relatively low potentials on the rockets, is the influence of the Earth's magnetic field on electron collection.

Classical theories predict that near large high-voltage probes, the ionospheric electrons are constrained more by magnetic field lines than attracted by the probe potential. This should result in a decrease in current from space-charge limited predictions that has yet to be observed in space. The Space Power Experiment Aboard Rockets I (SPEAR I) (W. J. Raitt et al., unpublished manuscript, 1988) was specifically designed to measure whether or not the Earth's magnetic field impedes electron collection. SPEAR I had two 10-cm radius spherical electron collectors each at the end of a 3-m boom. The planned experiment was to apply a positive voltage on the spheres, up to 46,000 V with respect to the rocket body, and measure the current of collected electrons from the ionosphere. In place of an electron beam, SPEAR I carried a plasma contactor on the bottom of the rocket to emit electrons and complete the circuit through the ionosphere. The plasma contactor was designed to keep the rocket body close to the same potential as the surrounding ionosphere. Consequently, most of the potential difference applied between the sphere and rocket body was intended to be dropped across a large electron-collecting sheath.

During the SPEAR I flight, the cover failed to come off the plasma contactor. Because of this, the plasma contactor was unable to expel the electrons collected by the spheres. The rocket body was driven thousands of volts negative to achieve current balance. Instead of a single, nearly spherical electron-collecting sheath around the spheres, a second, larger ion-collecting sheath was formed around the rocket body, partially enveloping the electron sheath. The structures and interactions between the two sheaths and the closure of the circuit through the ionosphere are the subjects of this paper. The basic theory of high-voltage objects immersed in a plasma is presented, followed by the results from detailed, three-dimensional calculations for the SPEAR I parameters. Both the flight results and the supporting calculations show that when the neutral gas pressure is low enough that ionization can be ignored, the sheath currents are small and are controlled by the geometry of the exposed high-voltage components.

EXPERIMENTAL ARRANGEMENT

The geometric arrangement of the booms and payload structure is shown in Figure 1. The 10-cm radius gold-plated spheres were mounted on bushings constructed with grading rings connected by resistors. The bushings produced a uniform potential gradient from the spheres to payload ground at the Y junction of the two bushings with the plastic support boom shown in Figure 1. The total resistance along each bushing

[1]S-Cubed Division of Maxwell Laboratories, La Jolla, California.
[2]Utah State University, Logan.
[3]Air Force Geophysics Laboratory, Hanscom Air Force Base, Massachusetts.
[4]University of Alabama, Huntsville.

Paper number 88JA03951
0148-0227/89/88JA-03951$05.00

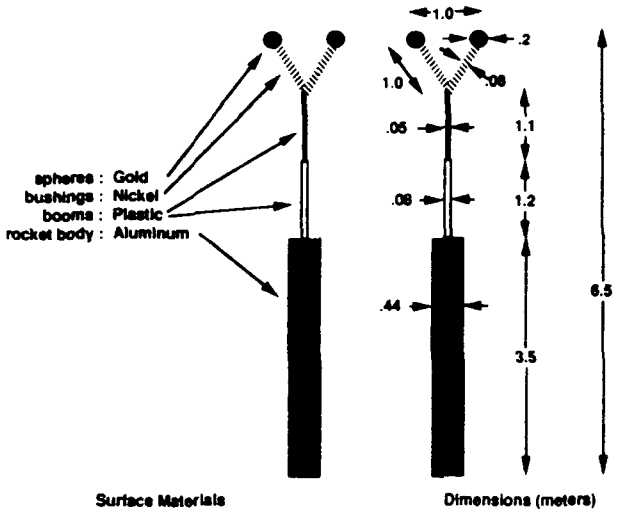

Fig. 1. The SPEAR I experiment. The rocket body was aluminum, the booms were plastic, the bushings were nickel, and the spheres were gold.

was 1 MΩ, and the number of rings used resulted in a potential drop of about 1 kV between each pair of rings when the sphere was at a potential of 46 kV. The rocket body was polished aluminum with a surface area of just over 5 m^2 and was connected to payload ground.

The voltage between the spheres and the payload ground was supplied from a charged 2.5-μF capacitor switched to the spheres by a high-voltage relay. A current-limiting resistor of 2 kΩ was connected in series with the capacitor. The electric schematic diagram of the high-voltage section for one sphere is shown in Figure 2. The fixed resistor of 700 kΩ in parallel with the bushing resistors of 1 MΩ resulted in a decay time constant of 1 s for the capacitor, ensuring that even in the absence of plasma currents, the applied potential would decay to near 0 V during the 5-s period for which the capacitor was connected to the sphere.

Figure 2 illustrates the two current monitors used to measure the total current from the capacitor and the current flowing down the graded bushing. The plasma current to the spheres was determined from the relation

$$I_{plas} = I_{tot} - I_{boom} = V/700 \quad (1)$$

where V is the measured voltage on the capacitor in kilovolts and the constant 700 is the constant fixed resistance connected between the capacitor and payload ground. An example of the plasma current to the sphere as a function of applied voltage is shown in Figure 3.

In addition to the high-voltage generating and monitoring instruments, the payload also contained diagnostics to monitor neutral pressure, ambient electron density and temperature, VLF and HF wave intensities, energetic ion and electron fluxes up to 30 keV, and optical imagery and photometry of glow in the vicinity of the spheres. A hollow cathode plasma contactor was also included in the payload with its plasma orifice at the end of the payload removed from the HV spheres.

SPEAR I was launched from NASA Wallops Flight Facility on December 13, 1987, at 2045 EST. It reached an apogee of 369 km at 351 s after launch. All of the results shown in this paper were taken within 10 km of 350 km. No significant altitude effect was observed between 120 and 320 km. The pressure measured during most of the high-voltage experiments ranged between 10^{-4} and 10^{-5} torr (J. Pickett and G. Murphy, private communication, 1988). This is significantly higher than the unperturbed ambient environment. During the last two high-voltage shots, the rocket was below 130 km and the background pressure was in excess of 10^{-4} torr. During these last shots, extensive ionization occurred and our calcula-

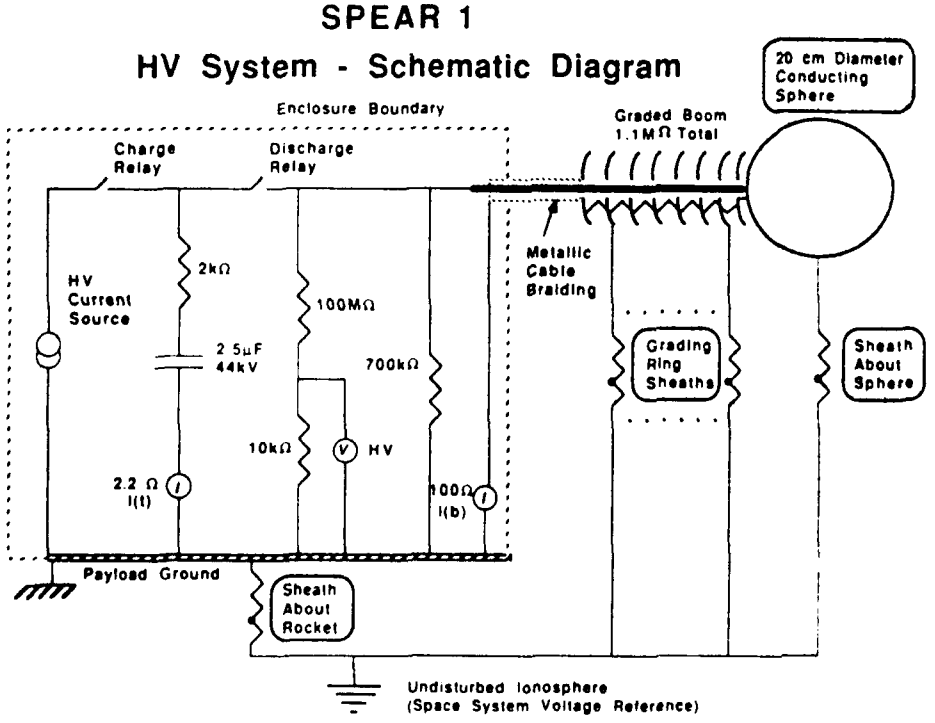

Fig. 2. The high-voltage circuit for one of the two spheres. Included are the two current monitors, $I(t)$ and $I(b)$.

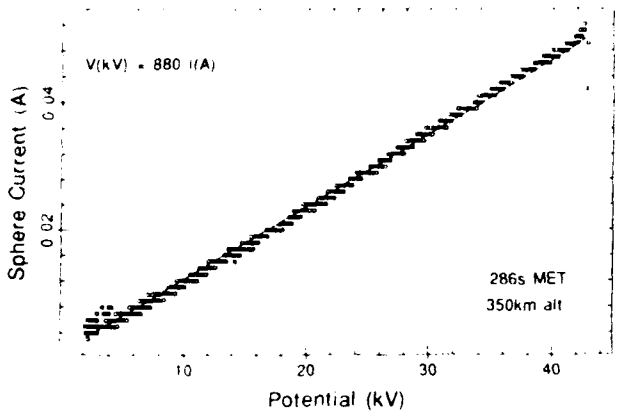

Fig. 3. The current versus voltage data where only one sphere was charged. These data were typical of all the higher-altitude shots.

tions do not apply. For most of the experiment, the rocket was oriented so that the Earth's magnetic field was perpendicular to the plane of the bushings and booms. During the later portion of the flight, the rocket was reoriented with respect to the magnetic field, but no effect was seen in the data.

The failure of the cap removal on the plasma contactor resulted in the payload ground being driven to high negative potentials as described earlier. The resulting ion flux from the ionospheric plasma to the vehicle was detected by the ion sensors of the energetic particle detectors. The ion flux energy spectra showed a high-energy cutoff which varied as the applied vehicle-sphere potential varied. The expected peak in the ion spectra was observed, but it was broader than expected from classical, collisionless acceleration of ionospheric ions through the vehicle charge sheath. Upper and lower bounds on the vehicle potential based on the spectral cutoff and peak energies are shown in Figure 4.

Further details on the instrumentation and examples of the flight data achieved can be found elsewhere (W. J. Raitt et al., unpublished manuscript, 1988).

Theory

The calculations presented depend on a few basic principles. First, a space charge sheath forms around the rocket surfaces which are at high potentials with respect to the surrounding ionospheric plasma. The size of the sheath is such that the net space charge in the sheath cancels the charge on the surfaces. Second, rocket components positive with respect to the ionospheric plasma collect electrons, and negative surfaces both collect ions and emit secondary electrons. Finally, charges flow between the SPEAR I rocket and the ionosphere in a complete circuit: the sum of the current from the positive surfaces is exactly balanced by the current to the negative surfaces. These basic principles control the time-averaged response between SPEAR I and the ionosphere.

A high-voltage capacitor in the SPEAR I rocket applied as much as 46,000 V between a 10-cm radius sphere and the body of the rocket. In a vacuum, applying this potential to an

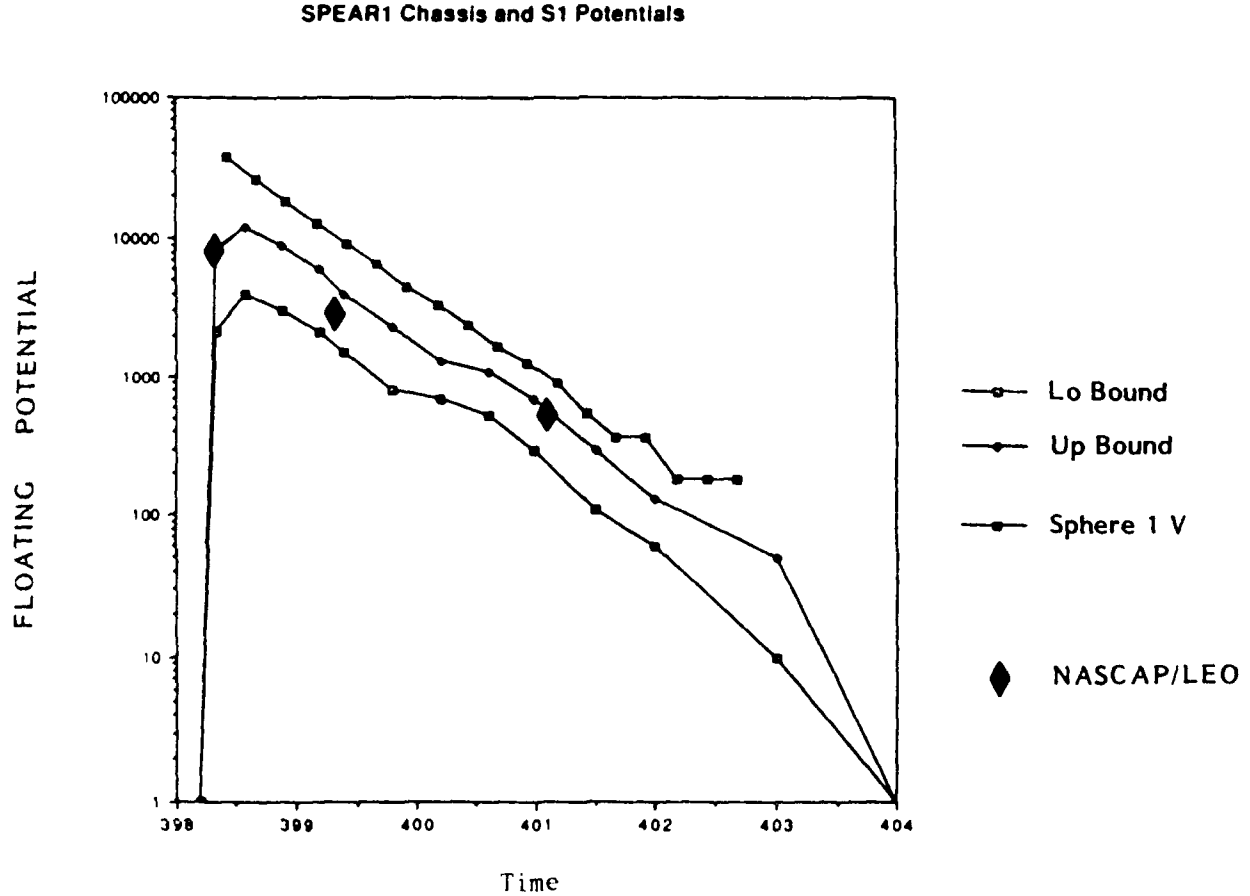

Fig. 4. The experimentally measured spacecraft ground potential as a function of time during one discharge of the capacitors. NASCAP LEO-predicted ground potentials are shown as diamonds on the curve.

isolated sphere would cause a charge of 5×10^{-7} C to appear on the surface. If immersed in a $n_e = 5 \times 10^{10}$ m^{-3}, $kT_e = 0.1$ eV plasma, typical of the ionosphere observed during the SPEAR I flight, the potential excludes ions from a substantial volume around the sphere. If the electrons were immobile, ions would be excluded from a 2.5-m radius volume surrounding the sphere ($(4\pi/3)R_s^3 n_i e = 4\pi\varepsilon_0 r\phi$). The space charge of the remaining electrons would balance the surface charge on the sphere. The transition from a quasi-neutral plasma to the complete exclusion of ions occurs in a few Debye lengths at the edge of this volume. On the scale of the volume radius, this is a very rapid transition. For the ion space charge to be significant, the local potential must be within a few kT_e of the ambient plasma potential. This is less than 10^{-4} of the applied potential during the SPEAR I flight. Under these conditions the sharp sheath edge approximation, i.e., the assumption that the transition between the quasi-neutral ambient plasma and the ion-free electron sheath is discontinuous, is accurate. This approximation is used in all of the calculations below.

When the electron response is included, the sheath radius expands. The self-consistent, space-charge-limited electron density and potential in the sheath surrounding a high-voltage spherical probe was first reported by *Langmuir and Blodgett* [1924]. The potential is obtained by solving Poisson's equation with the boundary conditions

$$\phi(a) = V$$
$$\phi(R_s) = 0 \qquad (2)$$
$$\left.\frac{\partial\phi}{\partial r}\right|_{r=R_s} = 0$$

where a is the sphere radius and R_s, the sheath radius, is found as an eigenvalue. The last equation results from Gauss's law when the space charge cancels the surface charge.

Plasma electrons enter at the sheath edge and are absorbed by the sphere. In steady state and without a magnetic field, current continuity and conservation of energy lead to an analytic expression for the space charge. This expression depends only on the radial position, the potential at that position, the sheath radius, and the current density entering the sheath.

$$n_e = J_s\left(\frac{R_s}{r}\right)^2\left(\frac{m_e}{2e\phi(r)}\right)^{1/2} \qquad (3)$$

Parrot et al. [1982] report that weak, long-range potentials in the plasma increase the current density entering the sheath to

$$J_s = 1.45 J_{\text{thermal}} \qquad (4)$$

where J_{thermal} is the one-sided plasma electron current density. This sheath current results when magnetic fields are neglected. No comparable results are available with magnetic fields. The calculations use (4) to relate the sheath edge current density to the plasma thermal current. The solution to Poisson's equation with the boundary conditions in (2) and the space charge density in (3) gives a sheath radius of 7.1 m.

The identical charge density could be found by solving the equations of motion for the electrons and integrating over the local distribution function. The analytical expression for space charge density [*Mandell and Katz*, 1983] is simpler to evaluate than integrating the equations of motion but is valid only when the geometry is symmetric and the magnetic field is so weak that it does not affect electron orbits. The analytical technique has been extended to more general geometries, but still without magnetic field effects. Calculation of densities from the equations of motion (e.g., following particle trajectories) is valid for all geometries and magnetic fields but is frequently hampered by numerical approximations and statistical noise. Both techniques are used in the calculations below. Analytical expressions are used in the bulk of the calculations, and to check those results, a few calculations were done by following electron trajectories.

In general, the sphere collects only a fraction of the electron current which enters the sheath. Even with no magnetic field, electron angular momentum can prevent sheath electrons from reaching the sphere. However, for the 46-kV potential and the plasma parameters being discussed, this is not a factor; all the 390-mA current entering the 7.1-m space-charge-limited sheath would be collected in the absence of a magnetic field. A magnetic field can reduce the current collected. Self-consistent, steady state calculations (M. J. Mandell et al., Current collection by a high-voltage sphere from a cold magnetoplasma, submitted to *Journal of Geophysical Research*, 1988) show that high-voltage spherical probes in ionospheric plasmas collect currents close to the limit derived by *Parker and Murphy* [1967]. The Earth's magnetic field of 0.4 G would reduce the collected current to only 14 mA from the 390 mA corresponding to the space-charge-limited value. According to recent estimates (P. Palmadesso, private communication, 1988), turbulence may cause cross-field transport and increase the collected current, but it would still be only a small fraction of the sheath current. The calculations of the current to the spheres presented here all include the effects of the magnetic fields on the electron trajectories. The magnetic field is particularly important for small rocket body potentials and large electron sheaths.

Around a negative sphere an identical sheath would form, but with space charge of the opposite sign. Ion motion is essentially unaffected by the Earth's magnetic field. When kilovolt ions impact aluminum oxide surfaces, they generate a large number of secondary electrons [*Dietz and Sheffield*, 1975]. For the high voltages experienced during the SPEAR I flight, each ion most likely produces more than 10 electrons. Secondary electrons produced by ion impact dominate the current to negative potential surfaces. However, since the electrons accelerated by the high fields travel more than 170 times as fast as O^+ ions, the ions still dominate the space charge density around a negatively charged object:

$$\frac{n_i}{n_e} \approx \left(\frac{I_i}{J_e}\right)\left(\frac{V_e}{V_i}\right) \approx \left(\frac{1}{10}\right)\left(\frac{170}{1}\right) \gg 1 \qquad (5)$$

The secondaries are accelerated along field lines, and almost all pick up too much angular momentum to be collected by the spheres. The calculations below include the current from ion-produced secondary electrons but ignore their contribution to the space charge.

Finally, when the spheres are biased positive with respect to the rocket body, the rocket body floats to a negative potential with respect to the plasma. It floats to the potential where the ion and secondary electron current to the body exactly balances the electron current collected by the spheres. The ionospheric plasma currents respond to a change of body potential on the time scale for a particle to transit the sheath: less than a microsecond for electrons and less than a millisecond for ions. In comparison, the voltage is applied to the spheres for a second. The floating potential response is so fast that at least

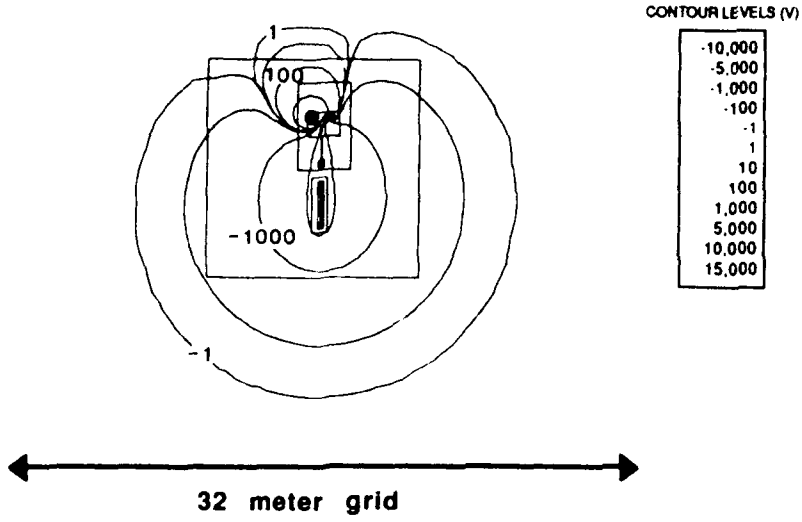

Fig. 5. POLAR 2.0 plasma sheath. The larger ion-collecting sheath partially engulfs the electron-collecting sheath.

in a time-averaged sense, the net current to SPEAR I must be zero.

While the elements of the theory presented here are not new, some components, particularly the mechanisms controlling electron collection from the ionosphere, have been at odds with data from lower-altitude rocket experiments. The calculations that follow show that all three elements (space charge sheaths, collected plasma currents, and current balance) are important in order to understand how the ionosphere responded to SPEAR I.

CALCULATIONS

The calculations presented below were performed to compare the flight measurements with the classical theories of electron collection from a magnetized plasma. The calculations were done using the NASCAP LEO and POLAR 2.0 computer codes which take account of the SPEAR I three-dimensional geometry as well as space charge and magnetic fields. While the experiment ideally would consist of spheres floating in space, the actual experiment, Figure 1, consists of two spheres supported by meter-long resistive bushings.

NASCAP LEO [*Mandell et al.*, 1982] and POLAR [*Cooke et al.*, 1985; *Lilley et al.*, 1986; *Katz et al.*, 1984] both solve Poisson's equation in three dimensions to determine the electric potential distribution in the plasma surrounding a spacecraft. They differ in that POLAR uses particle pushing to solve for the self-consistent space charge density by iteration, and NASCAP LEO uses space charge obtained from formulas based on current continuity in a homogeneous background plasma. Both codes use particle pushing to determine the plasma currents. Substantial testing has shown that in the absence of a magnetic field, the formulas in NASCAP/LEO have a wide range of applicability and can be as accurate as the particle pushing results. By using the analytical formulas, NASCAP LEO can find the sheath in less than one tenth the time of the self-consistent POLAR code. However, for the unusual geometries and strong magnetic effects seen in SPEAR I, it was necessary to perform self-consistent POLAR calculations for at least a few cases in order to assess the accuracy of the more approximate NASCAP LEO calculations.

Both codes use the sharp sheath edge approximation, which defines the sheath edge to be the potential contour beyond which the repelled species is entirely excluded. The Debye length for the F region ionospheric plasma is extremely short, of the order of a centimeter, and the sheath dimensions are large, of the order of tens of meters. The zone size at the sheath edge is of the order of half a meter. To compensate for the large zone size, the sheath boundary potential was taken to be 10 eV. The grid for both codes consisted of several embedded grids of progressively finer resolution. The finest grid resolution is 5 cm and is used to resolve the space around the spheres. Several calculations of current collection by a sphere were performed using the three-dimensional codes and compared with results from lower dimensional analyses. The two-dimensional simulations including a magnetic field performed for this comparison are discussed elsewhere (M. J. Mandell et al., Current collection by a high-voltage sphere from a cold magnetoplasma, submitted to *Journal of Geophysical Research*, 1988). The three-dimensional results are within 20% of the comparable two-dimensional calculations. For the cases in which magnetic fields are important, POLAR is in good agreement with the two-dimensional results, while NASCAP LEO makes errors as large as 50%. POLAR is able to correctly model the contraction of the sheath perpendicular to magnetic field due to $\mathbf{v} \times \mathbf{B}$ forces on electrons; the sheath NASCAP LEO calculates is unmodified by magnetic fields.

The same ionospheric plasma parameters, $n_e = 5 \times 10^{10}$ m^{-3}, $kT_e = 0.1$ eV, and $|\mathbf{B}| = 0.4$ G, were used in all the calculations. These parameters are consistent with the flight measurements. In both codes, plasma currents are calculated by tracking test particles in from the sheath edge until they hit the object or leave the sheath. The particles are subject to both electrical and magnetic forces. Owing to the magnetic field, a small fraction of the electrons neither leave the sheath nor are collected by the object even after extensive tracking. Our two-dimensional analysis has shown that self-consistent space charge contracts the sheath perpendicular to the magnetic field and reduces the number of apparently trapped particles and that these particles will eventually hit the object. In the SPEAR I calculations the number of trapped particles accounted for no more than 20% of the collected current. Neither counting them as collected nor discarding their contri-

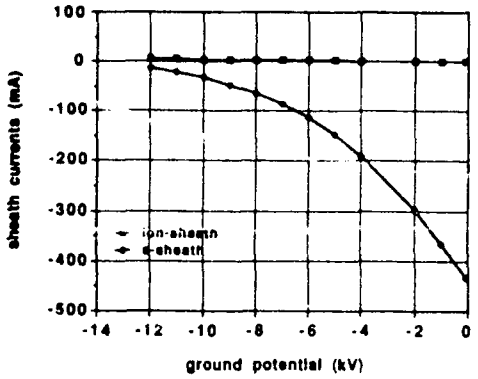

Fig. 6. Calculated ion and electron currents entering the sheath as a function of ground potential for the case where 46 kV is applied to one sphere

bution changes the results significantly; in the results below, they are always included in the collected current.

Ions produce large numbers of secondary electrons from aluminum oxide. Normally incident 10-keV oxygen ions were assumed to produce seven secondary electrons when they impact aluminum oxide. The most applicable data were for Na^+ on Al_2O_3. The value for O^+ was estimated from the Na^+ results of comparable ion velocity. Following Dietz and Sheffield the secondary yield γ was assumed to vary linearly with velocity:

$$\gamma = C(v - v_0) \tag{6}$$

where v_0 is the threshold velocity of 5.5×10^4 m s^{-1} and C is chosen to make the yield equal 7 for a 10-keV ion. The incident ions were assumed to hit isotropically, which increased the effective secondary yield by a factor of 2. The ion-generated secondary electron yield is the largest uncertainty in the calculations.

The calculations simulate the SPEAR I discharges when a single sphere was charged to the highest voltage and the voltage decayed owing to both the plasma currents and the current through a fixed resistor. The highest measured voltage on SPEAR I was 45,320 V; the calculations were done with voltages of up to 46,000 V. Four different applied voltages, 46, 24, 12, and 1 kV, were chosen to represent the sphere voltage during the discharge. For each sphere voltage a series of calculations was performed varying the potential of the rocket body with respect to the ionospheric plasma. For each of the rocket

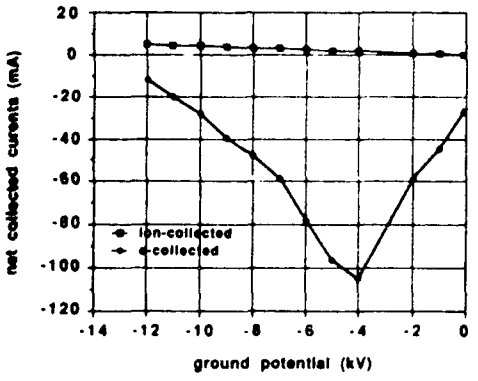

Fig. 7. Calculated ion and electron currents collected as a function of ground potential for the case where 46 kV is applied to one sphere.

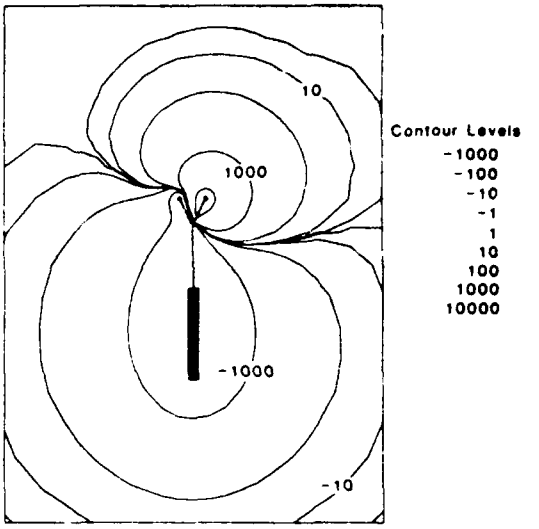

Fig. 8a. Potential contours calculated by NASCAP LEO for the case with one sphere biased to 46 kV and the spacecraft ground at −6 kV.

body potentials, NASCAP/LEO calculated the ion and electron plasma sheaths along with the current to the rocket. The equilibrium rocket body floating potential was determined by balancing the electron current to the sphere with the secondary electron-enhanced ion current to the rocket body. This set of calculations thus yields both the potential on the rocket body and the current to the sphere. Calculations using the POLAR code were performed for 46 kV on the sphere and both −6 kV and −8 kV on the body. These calculations

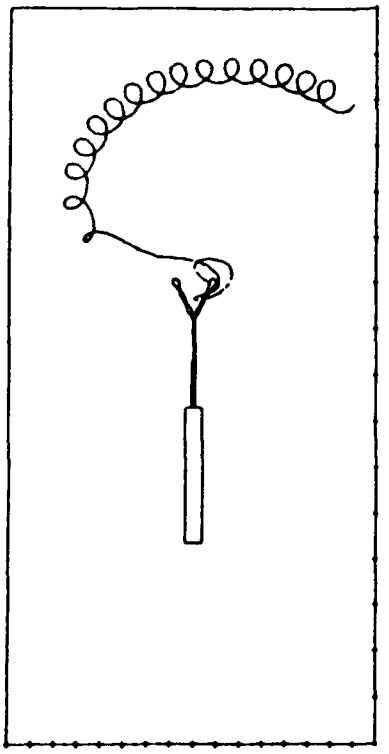

Fig. 8b. Path of an electron in the potentials shown in Figure 8a. Note that the path is dramatically influenced by the presence of the ion-collecting sheath.

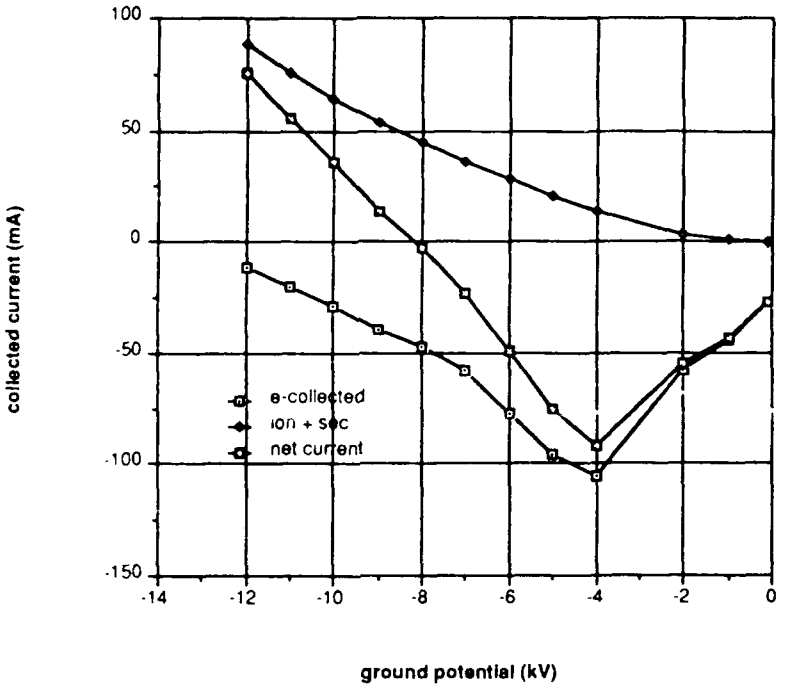

Fig. 9. Currents collected as a function of the ground potential including the effects of secondaries and the presheath enhancement for the case where 46 kV is applied to one sphere.

showed that for these interacting bipolar sheaths, NASCAP LEO, which uses space charge formulas, gives almost the same results as POLAR, which uses space charge found from self-consistent particle tracking. For a rocket body potential of -8 kV, the collected electron current by the sphere is 47.6 mA (NASCAP LEO), compared with 53.4 mA (POLAR). The collected ion current by the rocket body is 3.3 mA (NASCAP LEO) compared with 3.1 mA (POLAR). When ion-generated secondary electrons are accounted for, the floating rocket body potential for current balance from both NASCAP LEO and POLAR is -8.3 kV.

Results

The ion-collecting sheath surrounding the rocket body dominates the smaller electron-collecting sheath around the sphere. As is shown in Figure 5, even though the body potential is only a small fraction of the sphere potential, the much larger sheath forms because the surface charge on the 5-m^2 rocket body is much greater than the charge on the 0.04-m^2 sphere. This is only due to their relative sizes. The effect of the large ion-collecting sheath is to pinch off the electron-collecting sheath and to reduce the area through which electrons can enter from the ionosphere. As the rocket body becomes more negative, the ion-collecting sheath grows until it completely isolates the electron-collecting sheath from the ionosphere. Figure 6 shows the ionospheric electron thermal current entering the sheath as a function of the rocket body potential when 46 kV is applied to the sphere. For rocket body potentials more negative than -15 kV, the ion-collecting sheath completely surrounds the positive sheath, preventing any electrons form entering the sheath. This is a lower bound on the body potential and doesn't depend on magnetic field effects on electrons nor on the yield of ion-generated secondary electrons.

While the electron current entering the sheath decreases monotonically as the body floats negative, the electron current collected demonstrates a more complicated dependence on the body potential (Figure 7). For small body potentials, the electron current collected by the sphere actually increases as the current into the sheath decreases. The magnetic field reduces the collected electron current to a small fraction of the current entering the sheath. However, as the body potential becomes negative, it forms an ion-collecting sheath which distorts the symmetry of the electron-collecting sheath. This distortion enables electrons entering the sheath to $\mathbf{v} \times \mathbf{B}$ drift into regions of strong electric field, from which they can be collected (Figure 8). As the body potential varies from 0 to -4 kV, the fraction of electrons collected increases faster than the electron sheath area decreases. For large negative body potentials, most of the current entering the sheath is collected, and the net electron current collected decreases because the sheath area decreases. The potential where the collected electron current starts to decrease as the sheath decreases provides another bound on the body floating potential. This bound does not depend on the yield of ion-generated secondary electrons but depends critically on the effects of the magnetic field on electron motion.

TABLE 1. Body Potential and Plasma Current Versus Sphere Bias

Sphere Bias, kV	Body Potential, kV	Current, mA
+46	−8.3	45.2
+24	−3.3	26.9
+12	−3.3	13.4
+1	0.6	1.4

Values are as calculated by NASCAP/LEO.

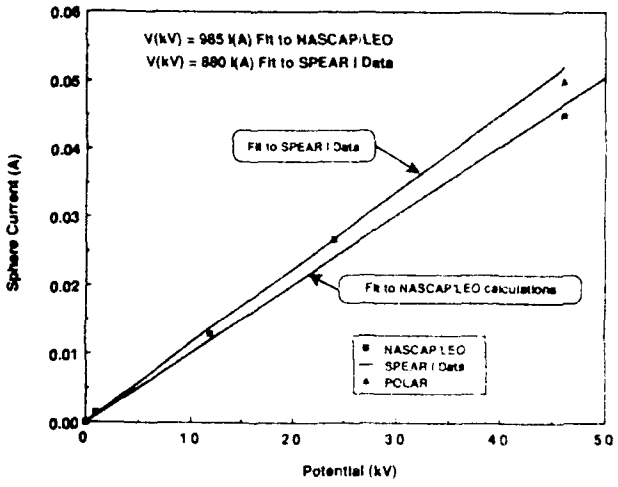

Fig. 10. Observed and calculated current collected by the 46-kV sphere as a function of applied potential.

The rocket body floats to a potential between these two bounds, depending on the secondary electron yields. Since the model for the secondary electron yields that was presented in the preceding section contains a large uncertainty, it is important to consider the sensitivity of the results to the yields. The three-dimensional calculations can be used to determine body potentials and currents as a function of the secondary electron yields. For the system with 46 kV applied that we have been considering, a yield of 30 is necessary to produce an equilibrium body potential of −6 kV with a current of 78 mA, while a yield of 3 corresponds to a potential of −11 kV and a current of 20 mA. Thus while the results are dependent on the assumed secondary electron yields, extremely large changes in these yields are necessary to produce qualitative changes in the potentials and currents. The three-dimensional sheath calculations that have been performed can be used with more accurate yield data if they become available to remove this uncertainty. Figure 9 shows the current to the body including secondary electrons and the electron current to the sphere. Also plotted is the net current to SPEAR I. The zero in the net current determines the body floating potential. When 46 kV is applied to the sphere, the calculated floating potential is −8.3 kV with a current of 45 mA.

Table 1 shows the calculated floating potentials and sphere currents for four sphere bias voltages. In Figure 10 the sphere currents are compared with a fit to the flight data. Also shown is a line through the origin fit to the four calculated points. A straight line also fits the flight data. The straight line through the calculated current-voltage points provides an effective "resistance" which can be compared with the same quantity from the flight data. The apparent linearity of the current-voltage relationship is peculiar to the SPEAR I configuration and the voltage range of the calculations. The agreement between the calculations and experiment is well within the estimated uncertainty of the calculations, which is about 30%. Figure 4 shows the calculated floating potentials compared with bounds determined from ion spectral measurements made during flight. As discussed earlier, the spectra were much broader than anticipated, possibly as a result of backscatter from the rocket body or from sheath oscillations. The calculations all fall within the experimental bounds.

Discussion

SPEAR I measured the response of the ionospheric plasma to large objects with exposed high voltages. The rocket flew high enough and released little enough neutral gas that ionization within the sheath did not cause the high-current, low-voltage glow discharges observed on low-altitude electron beam rockets and also observed during large chamber testing of SPEAR I. The calculated floating potentials and currents collected are in agreement with potentials and currents measured during the flight. That the most important physical processes are included in the calculations is supported by the close agreement between the calculations and the experiment in such a complicated system. High-impedance space charge sheaths were maintained until the rocket passed below 130 km in altitude, where ionization effects become dominant.

Acknowledgments. The authors wish to acknowledge useful discussions with members of the SPEAR I theory group under the direction of Dan Alfred, in particular, John Antoniades, Eric Kunhardt, and Peter Palmadesso. This work was sponsored in part by the Air Force Geophysics Laboratory under AFGL 19628-86-C-0056.

The Editor thanks K. N. Erickson and J. P. Lebreton for their assistance in evaluating this paper.

References

Beard, D. B., and F. S. Johnson, Ionospheric limitations on attainable satellite potential, *J. Geophys. Res.*, *66*, 4113, 1961.

Chen, F. F., Electric probes, in *Plasma Diagnostic Techniques*, edited by R. H. Huddlestone and S. L. Leonard, pp. 113–200, Academic, Orlando, Fla., 1965.

Cooke, D. L., I. Katz, M. J. Mandell, and J. R. Lilley, Jr., Three-dimensional calculation of shuttle charging in polar orbit, in *Spacecraft Environment Interactions Technology—1983*, *AFGL-TR-85-0018*, *NASA CP-2359*, p. 205, Air Force Geophysics Laboratory, Hanscom Air Force Base, Mass., 1985.

Dietz, L. A., and J. C. Sheffield, Secondary electron emission induced by 5–30-keV monatomic ions striking thin oxide films, *J. Appl. Phys.*, *46*, 4361, 1975.

Katz, I., D. E. Cooke, D. E. Parks, M. J. Mandell, and A. G. Rubin, Three-dimensional wake model for low Earth orbit, *J. Spacecr. Rockets*, *21*, 125, 1984.

Laframboise, J. G., and J. Rubinstein, Theory of a cylindrical probe in a collisionless plasma, *Phys. Fluids*, *19*, 1900, 1976.

Lai, S. T., H. A. Cohen, K. H. Bhavnani, and M. Tautz, Sheath ionization model of beam emissions from large spacecraft, *Spacecraft Environmental Interaction Technology—1983*, *AFGL-TR-85-0018*, *NASA CP-2359*, p. 253, Air Force Geophysics Laboratory, Hanscom Air Force Base, Mass., 1985.

Langmuir, I., and K. B. Blodgett, Currents limited by space charge between concentric spheres, *Phys. Rev.*, *24*, 49, 1924.

Lilley, J. R., Jr., I. Katz, and D. L. Cooke, $v \times B$ and density gradient electric fields measured from spacecraft, *J. Spacecr. Rockets*, *23*, 656, 1986.

Machlum, B. N., J. Troim, N. C. Maynard, W. F. Denig, M. Friedrich, and K. M. Torkar, Studies of the electrical charging of the tethered electron accelerator mother-daughter rocket MAIMIK, *Geophys. Res. Lett.*, *15*, 725, 1988.

Mandell, M. J., and I. Katz, Potentials in a plasma over a biased pinhole, *IEEE Trans. Nucl. Sci.*, *NS-30*, 4307, 1983.

Mandell, M. J., I. Katz, and D. L. Cooke, Potentials on large spacecraft in LEO, *IEEE Trans. Nucl. Sci.*, *NS-29*, 1584, 1982.

Mott-Smith, H. M., and I. Langmuir, The theory of collectors in gaseous discharges, *Phys. Rev.*, *28*, 727, 1926.

Parker, L. W., and B. L. Murphy, Potential buildup on electron-emitting ionospheric satellites, *J. Geophys. Res.*, *72*, 1631, 1967.

Parrot, M. J. M., L. R. O. Storey, L. W. Parker, and J. G. Laframboise, Theory of cylindrical and spherical Langmuir probes in the limit of vanishing Debye number, *Phys. Fluids*, *25*, 2388, 1982.

Rubinstein, J., and J. G. Laframboise, Upper bound current to a cylindrical plasma probe in a collisionless magnetoplasma, *Phys. Fluids*, *21*, 1655, 1978.

Rubinstein, J., and J. G. Laframboise, Theory of a spherical probe in a collisionless magnetoplasma, *Phys. Fluids*, *25*, 1174, 1982.

Rubinstein, J., and J. G. Laframboise, Theory of axially symmetric probes in a collisionless magnetoplasma: Aligned spheroids, finite cylinders, and disks, *Phys. Fluids*, *26*, 3624, 1983.

Winckler, J. R., The application of artificial electron beams to magnetospheric research, *Rev. Geophys.*, *18*, 659, 1980.

D. L. Cooke, Air Force Geophysics Laboratory, Hanscom Air Force Base, MA 01731.

V. A. Davis, A. Jongeward, I. Katz, R. A. Kuharski, J. R. Lilley, Jr., and M. J. Mandell, S-Cubed, P.O. Box 1620, La Jolla, CA 92038.

G. Larson, D. Rau, and R. B. Torbert, University of Alabama, Huntsville, AL 35899.

W. J. Raitt, Utah State University, Logan, UT 84322.

(Received May 17, 1988;
revised October 24, 1988;
accepted October 27, 1988.)

JOURNAL OF GEOPHYSICAL RESEARCH, VOL. 94, NO. A7, PAGES 8965-8976, JULY 1, 1989

The POLAR Code Wake Model: Comparison With in Situ Observations

G. MURPHY

Jet Propulsion Laboratory, Pasadena, California

I. KATZ

S-Cubed, La Jolla, California

Measurements of the ion and electron densities associated with the wake of the shuttle orbiter were made by the Plasma Diagnostics Package (PDP) during the 1985 Spacelab 2 mission. Cross sections of the wake at distances of 50–250 m downstream and measurements along the wake axis from 5 to 100 m were obtained. The POLAR wake model, developed for The Air Force Geophysics Laboratory to study charging of spacecraft in low-altitude high-inclination orbits, was used to perform a three-dimensional simulation of the plasma wake evaluated at points along relative trajectories of the PDP. The POLAR code uses several simplifying assumptions to predict wake densities. These include neglecting the magnetic field and assuming that the plasma is quasi-neutral. The code models plasma density ahead of the expansion front using a neutral approximation, and models the plasma density behind the expansion front by using the self-similar solution of the expansion of a plasma into a vacuum. For cases where $T_e \gg T_i$, the front is not sharp and thermal motion can account for most of the expansion. This approach is computationally very efficient. The results presented here are the first known comparison between such a model and actual *in situ* data obtained for objects of scale size 10^1 m. Excellent qualitative and quantitative agreement are found at distances greater than 30 m, indicating that at least to first order, the model approximations are justified. An anticipated disparity between the model and data suggests that the orbiter's near wake may be filled predominantly by ion pickup ion population created from neutral contaminants, and that these would have to be included in accurate wake models of large gas-emitting objects are required.

INTRODUCTION

In this paper we discuss measurements made by the Plasma Diagnostics Package (PDP) during Spacelab 2, which are presented by *Murphy et al.* [1989], and compare those results with predictions from the Air Force Geophysics Laboratory (AFGL) POLAR wake code, which uses a complex geometric model of the orbiter and the self-similar solution of the expansion of a plasma into a vacuum as its model basis. Previous reports [*Katz et al.*, 1985] have compared the predictions of POLAR to observations of $T_e \approx T_i$ plasmas in the laboratory.

Caution should be exercised in extending conclusions about the accuracy of the POLAR model to conclusions regarding verification of the underlying physical processes it contains. Several other investigations have studied the applicability of the self-similar mathematics [*Samir et al.*, 1983; *Raychaudhuri et al.*, 1986; *Gurevich et al.*, 1969; *Diebold et al.*, 1987; *Kozima et al.*, 1988] to wakes. It is our purpose only to determine if POLAR provides a reasonable model for the wakes of "large" objects in the ionosphere, as it has for $T_e \approx T_i$ plasmas in the laboratory.

We describe briefly the POLAR model and review the physics it contains, compare the data with the model, and then discuss the range of validity of the code.

THE POLAR CODE

To develop a code that can adequately describe the plasma wake behind a large object, particularly one of complex geometry, careful consideration of assumptions and approximations are required, as are simplifications allowing for computational efficiency. The POLAR code has evolved with such considerations in mind. A detailed description of the POLAR wake model is given by *Katz et al.* [1985], and it is the purpose here only to review the basic physics and processes in POLAR so the reader may have some insight into the validity of the code.

The model of the wake structure used by POLAR depends on the position relative to the so-called ion front. This ion front marks the boundary where electron density begins to change on a scale commensurate with the Debye length and the ion density takes a sudden and dramatic drop. Several authors have discussed the relationship between the wake fill process and the theoretical problem of the expansion of a plasma into a vacuum. In particular, problems applicable to ionospheric conditions have been treated by *Gurevich et al.* [1966], *Gurevich and Pitaevskii* [1975], and *Singh and Schunk* [1982], to name a few.

The solution to the Vlassov-Poisson equation system is in general quite difficult to obtain, but for the expansion of a plasma into the void it can be solved explicitly [*Gurevich et al.*, 1969]. Ahead of the ion front the plasma is treated as rarefied; its motion is controlled by the thermal spread in ion velocities. Behind the front the motion is controlled by the electron temperature and ion mass. Figure 1 illustrates these regimes and defines the coordinate system used.

The governing equations in the region behind the front, considering that electrons are more mobile than ions and that they maintain equilibrium with a local potential, are

The Boltzman relation

$$n_e = n_0 \exp(e\phi/kT_e) \quad (1)$$

Paper number 89JA00582
0148-0227/89/89JA-00582$05.00

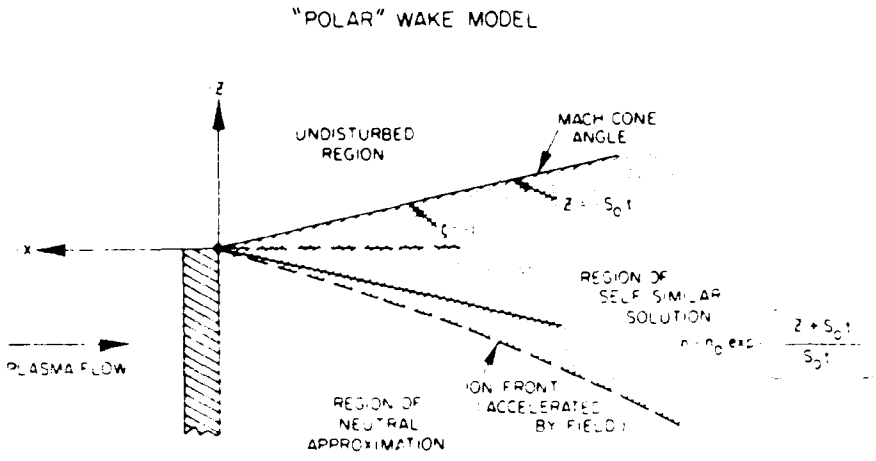

Fig. 1. The POLAR wake code distinguishes three regions of interest. The ambient plasma, the region of self-similar model, and the neutral approximation spaces are bounded by the Mach cone $Z = -S_0 t$ and ion front respectively. The coordinate system used is consistent with equations (1) through (10).

Continuity

$$\frac{\partial n_i}{\partial t} + \frac{\partial (n_i v)}{\partial z} = 0 \tag{2}$$

Equation of motion

$$\frac{\partial v}{\partial t} + v\frac{\partial v}{\partial z} = -\frac{e}{M}\frac{\partial \phi}{\partial z} \tag{3}$$

Poissons equation

$$\frac{\partial^2 \phi}{\partial z^2} = 4\pi e(n_i - n_e) \tag{4}$$

where

n_0 ambient density,
n_i ion density,
n_e electron density,
T_e electron temperature,
e electron charge,
ϕ local potential,
k Boltzman's constant

and where z is a variable representing distance parallel to the front velocity or, in this case, perpendicular to the orbital velocity.

Crow et al. [1975] have numerically solved (1) through (4) to predict the position of the ion front. *Katz et al.* [1985] developed an analytical fit to the Crow results

$$Z_f(t) = 2\lambda_D \left\{ \left(\omega t + \frac{1}{\alpha}\right) \ln\left(1 + \alpha\omega t\right) - \omega t \left(1 - \frac{0.429}{\alpha}\right)\left(\omega t - \frac{1}{\alpha}\ln\left(1 + \alpha\omega t\right)\right) \right\}^{1/2} \tag{5}$$

where

$$\omega = \frac{(4\pi n_{i0} e^2)^{1/2}}{M}, \qquad \lambda_D = \frac{(kT_e)^{1/2}}{4\pi n_{i0}},$$

are the ion plasma frequency and Debye length, respectively, and α is a free parameter determined to be 1.6.

Katz et al. [1985] showed that this formula agrees well with laboratory data from *Wright et al.* [1985] and incorporated it in POLAR. Ahead of this front Z_f, the plasma is assumed to expand owing to thermal motion, the so-called "neutral approximation." Behind Z_f, the plasma evolves into a state which is self-similar [*Chan et al.*, 1984]. The self-similar solution of (1)–(4) for $z > -S_0 t$ is

$$n = n_0 \exp\left[-\frac{z + S_0 t}{S_0 t}\right] \tag{6}$$

where $S_0 = (kT_e/M)^{1/2}$ is the ion acoustic speed.

The time variable is defined as

$$t = \frac{x}{V_0} \tag{7}$$

where x is the distance behind the object (perpendicular to z) and V_0 is the orbital velocity. We define the self-similar variable ζ as

$$\zeta = \frac{z}{S_0 t} \tag{8}$$

Thus the self-similar solution essentially states that between the region bounded in positive z by the front Z_f and in negative z by the line $z = -S_0 t$, the density rises exponentially to be equal to the ambient value along $z = -S_0 t$. This is an intuitively reasonable result.

In summary, the wake routines in POLAR employ two limiting cases: (1) Ahead of the ion front the electric field is negligible and the motion of ions is identical to neutrals. (2) Behind the ion front, whose position is determined by (5), the quasi-neutral self-similar solution of (6) is implemented.

POLAR has routines which model accurately the geometry of the object, and the "neutralization" trajectories are calculated from

$$f(\mathbf{x}, \mathbf{v}) = f_0(\mathbf{x}, \mathbf{v})\,\Omega(\mathbf{x}, \mathbf{v}) \tag{9}$$

where $f_0(\mathbf{x}, \mathbf{v})$ is the unperturbed distribution function for a drifting Maxwellian, and $\Omega(\mathbf{x}, \mathbf{v})$ has value 1.0 if a ray starting from $\mathbf{x}$ and going in the direction $\mathbf{v}$ would strike the vehicle and 0.0 if it would not.

FIG. 2. Using the relative trajectory of the PDP and orbiter, POLAR calculates the density as a function of time for the entire wake transit time period. Areas of interest are labeled in the figure. The assumed normalization values for the plasma are $n_\infty = 1 \times 10^6$ cm^{-3} and $T_\infty = 2500$ K.

The local density is given by

$$n(\mathbf{x}) = \int_{\Omega_1} f(\mathbf{x}, \mathbf{v}) \, d\Omega_1 = \int_{\Omega_2} g(\mathbf{x}, \Omega_2) \left\{ \int_0^\infty f(\mathbf{x}, \mathbf{v}, \Omega_2) v^2 \, dv \right\} d\Omega_2 \quad (10)$$

This initial density calculated in three dimensions for neutral particles is compared with density calculated assuming the complex geometric object is replaced by a flat plate at a position where the dominant source appears at the object edge. This ratio provides a "geometric correction factor," which is applied to the quasi-neutral one-dimensional solution discussed earlier for positions behind Z_f. In this way, POLAR can calculate quite rapidly an approximate value for the ion and electron densities in the wakes of complex objects.

Note that the assumptions behind the front are (1) that the electron temperature and ion mass govern the equation of motion, (2) that the plasma is quasi-neutral, (3) that the magnetic field does not affect the ion or electron motion, (4) that equation (5) serves as a good approximation for determining the boundary of the ion front, and (5) that the geometric correction factor calculated in detail with the three-dimensional neutral model can be approximately applied to correct the plasma densities as well. Therefore the algorithm can address complex geometries but takes advantage of the smooth wake structure characteristic of ionospheric plasmas where $T_i / T_e \ll 1$. Additionally, the model ignores fields existing in a sheath near the body surface, which should not be of concern in our case where the orbiter is near plasma potential. This implies that ion acceleration calculated by POLAR is dominated by electric fields due to space charge separation in the wake.

Comparison of Results

Figure 2 is a plot of the normalized density as a function of time predicted by POLAR for the PDP/orbiter relative trajectory. The density ratio $N_{wake}/N_{ambient}$ varies from approximately 0.9 for wake transit (WT) 1, which is at a distance of 245 m, to 0.2 for the closest, WT 3, at 45 m.

One must be careful when comparing the model to the data, since the model assumes a fixed background density of 10^6 cm^{-3}, whereas the actual ionospheric density can and does vary considerably. The background density chosen for the model is typical of that observed in the F1 ionosphere. The assumed model temperature is also a constant 2500 K. The observed temperature varies plus or minus 25% from this assumed value during times of interest. The wake transits were all planned to occur in the relatively stable dayside ionosphere, and over the time span of a given wake transit the background density is believed to be stable to ±10% [*Murphy et al.*, 1989]. In the following discussion we will always compare the observed density ratio during a wake transit to the percentage change predicted by the model.

Figure 3*a* plots the observed electron and ion density depression during the back-away maneuver, with a constant 10^6 cm^{-3} as the reference density [*Murphy et al.*, 1989]. The density chosen for normalization is arbitrary and does not affect the shape of the profile as long as it is constant. It is the shape and relative depth of the profile we wish to compare with POLAR. The dots in Figure 3*a* are the electron density (small periodic depressions result when the boom-mounted probe passes through the wake of the spinning PDP). The plus symbols are the ion density obtained once per spin cycle. During the back-away, the PDP and orbiter pass from a latitude of approximately −29° to −30° in early afternoon local time. Figure 3*a* also shows the predicted normalized density calculated by the POLAR model described earlier. As can be seen, good agreement exists at distances from −50 to −75 m. It should also be noted that over the range of the data shown, the RPA and LP data agree on density within ±30%.

As discussed by *Murphy et al.* [1989], we cannot easily normalize to either the previous or following orbit, so we use a constant value of 10^6 cm^{-3} for $N_{ambient}$. This value appears to be the peak density observed after the PDP has left the wake approximately 1 hour and 40 min later. Over the relatively long period of this maneuver, the ionosphere has surely changed by more than 10%, and this may explain the disparity after $t = -20$ min, since the PDP to orbiter distance is changing relatively little. Figure 3*b* is a plot of the predicted density calculated by the IRI ionosphere model and the measured density one orbit later (same local time and latitude). Note that the gradual variations observed owing to changing local time and latitude are consistent with the general trend predicted by the IRI model.

Let us turn now to the wake transit observations. Table 1 lists the wake transits and compares the predicted and observed depletions as well as conditions at the time of the center of the wake. Note that in this entire range of −50–250 m, the calculations and observations agree to within ±30%.

Since the orbiter has a complex geometry, the details of the wake structure at a distance of 45 m (WT 3) downstream may be affected. Figure 4 plots a detail of that wake transit and the POLAR model as a function of time. The data are normalized to a constant value, since it is clear some variation in background density occurs but it is not clear exactly what that variation is. To normalize to any unknown value other than a constant would introduce artificial variation and skew the results. *Murphy et al.* [1989] discuss this issue in detail and in that case, WT 3 is normalized by the data from the prior orbit. However, *Murphy et al.* [1989] are attempting no comparison to a model. During this wake transit the background is believed to vary by as much as 10%

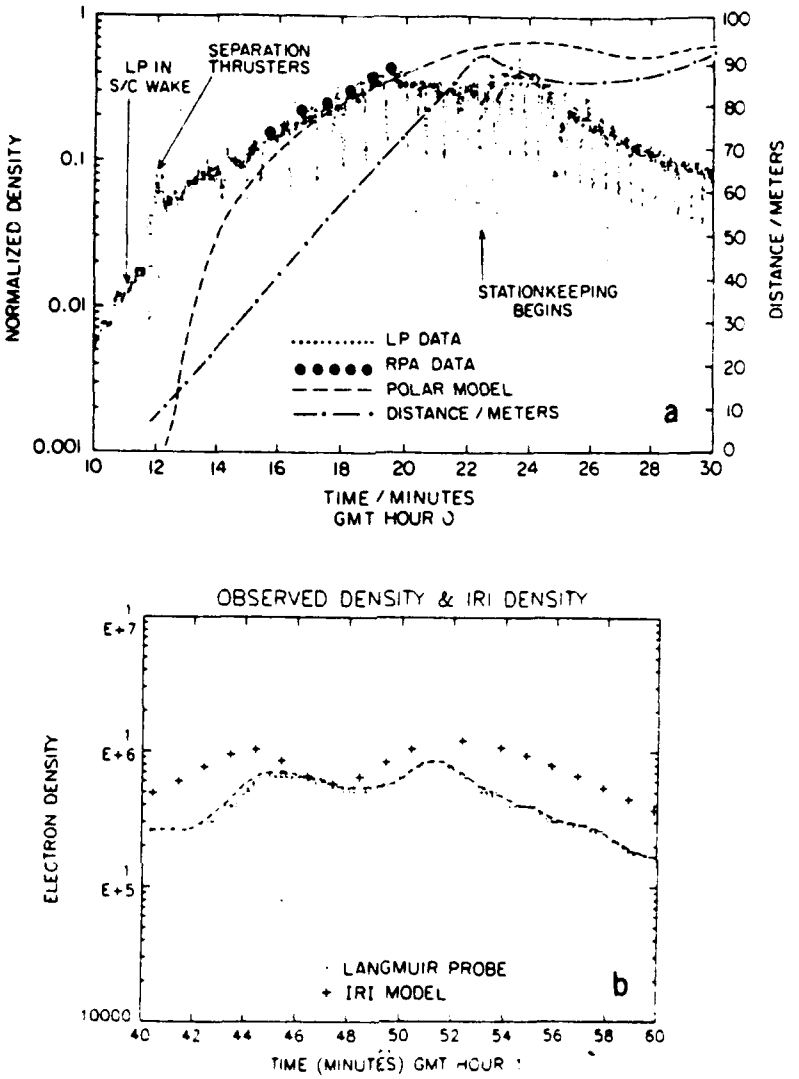

Fig. 3. Ion and electron data during the back-away are plotted in Figure 3*a*, normalized to $n_e = 1 \times 10^5$ cm^{-3}. Note the relatively good agreement between model and data between 30 and 75 m. Beyond $t = 20$ min (75 m) background density varies considerably, as is illustrated in Figure 3*b*, which includes data for one orbit later than Figure 3*a* at approximately the same station-keeping position, superimposed on a predicted density for this orbit from the IRI ionosphere model.

[*Murphy et al.*, 1989] so the model cannot be tested to an accuracy greater than that.

Discussion

In examining the back-away density profile, we find three relevant observations from Figure 3.

1. Close to the orbiter (<30 m) the model underestimates the observed density by 1 to 2 orders of magnitude.

2. In the range 30–75 m the model predicts quite accurately the gradual increase in density until the time $t = 20$ min. (Figure 3). After $t = 20$ min the observed density seems to have a variation, which is not believed to be wake-related. These density changes result from ionospheric variability as the spacecraft approaches the dawn-dusk meridian plane and are predicted by empirical models such as IRI.

Considering the first observation, recall that the assumptions incorporated within the POLAR wake model require a quasi-neutral plasma, assume a self-similar solution, and neglect magnetic fields. Since the electron and ion densities observed even at the beginning of the release and back-away period agree within 10%, it would seem that quasi-neutrality would be valid. It has been shown by *Chan et al.* [1984] that after a few ion plasma periods (≈0.1 ms in this case) the plasma expansion becomes self-similar. For the case of the shuttle orbiter, this takes place within the first ≈1 m of the wake. The magnetic field, if it is to be considered for this

TABLE 1. Comparison of Observations From *Murphy et al.* [1989] With POLAR Predictions

Wake	Latitude deg	T_e K	Distance m	POLAR Normalized Density	Observed Normalized Density
1	35	2500	242	0.9	0.80
2	45	3000	125	0.75	0.61
3	−10	1500	45	0.20	0.18
4	−35	2000	105	0.65	0.90

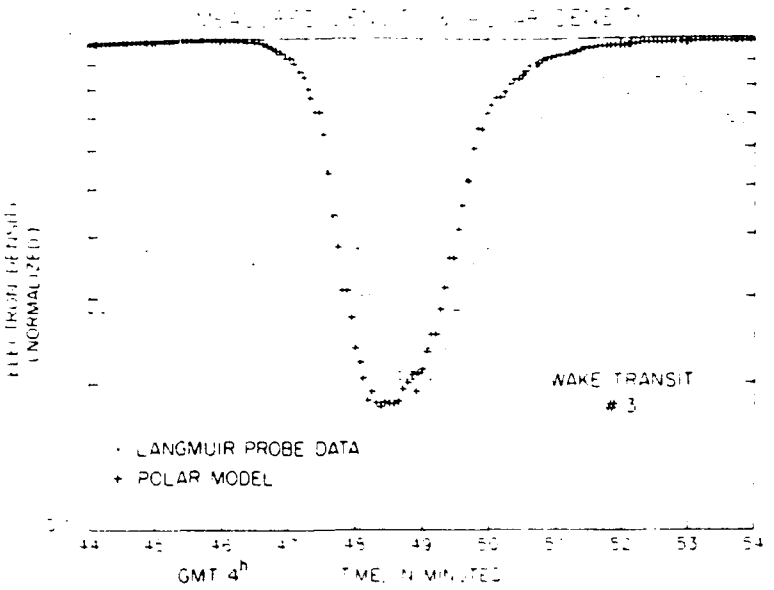

Fig. 4. Detail of data from WT 3 is compared to POLAR predictions. Data are normalized to a constant. Since there may be variation in background of ~10%, differences of that order between data and model are not significant.

case, would always act to limit plasma flow, rather than enhance it. Therefore it too can be eliminated from serving as an explanation for the poor fit at less than 30 m.

The answer to the disparity between model and observation would seem to lie in the role played by contaminant ions. *Murphy et al.* [1989] discuss these ions and offers their presence as an explanation for the disparity between these data and that taken at similar distances while on the remote manipulator system (RMS).

Let us turn now to the 30- to 75-m distance region. The most dominant characteristic of both the data and model is the relatively smooth increase in density as the PDP moves axially along the orbiter wake.

This midwake region has been studied extensively in the laboratory and the wake-fill process depends strongly on the body size, body potential, and ratio of ambient ion to electron temperature. *Stone* [1981], *Fournier and Pigache* [1975], *Hester and Sonin* [1970], and many others have performed laboratory experiments and observed fine structure in wakes, including ion density peaks along the wake axis and wavelike condensation disturbances. It is important, however, to note that for the case of large bodies in low earth orbit (LEO) (1) the body potential is not too different from the plasma potential (a few kT_e at most, since the body surface is an insulator and does not expose $\mathbf{v} \times \mathbf{B}$ potential to the plasma), (2) the plasma is a cold Maxwellian (Lev) and collisionless, and (3) the ambient ion and electron temperatures are close to being equal.

An excellent review of laboratory work before 1975 is given by *Fournier and Pigache* [1975]. Another excellent review of the subject of expansion of plasma into the wake is given by *Samir et al.* [1983]. In these cases the authors agree with the basic finding of *Gurevich and Pitaevskii* [1969] that the fine structure and ion peaks observed in certain laboratory investigations vanish as T_i approaches T_e. We see in this case that in spite of (or perhaps because of) the effect of contaminant ions, we have a large-scale wake which is basically devoid of any fine structure, at least in the sense of total electron or ion density. It should be emphatically noted, however, that this does not imply knowing all there is to know about the wake structure. The overall plasma density is only the zeroth order parameter. Ion and electron composition [*Grebowsky et al.*, 1987]; vector measurements of ion velocities [*Stone et al.*, 1983, 1988]; electron temperature [*Murphy et al.*, 1986; *Raitt et al.*, 1984]; plasma turbulence [*Raitt et al.*, 1984] all play roles in understanding the total physics of the wake structure for such a complex, gas-emitting, large object.

As discussed earlier, the structural differences between predictions and observations after $t \approx 20$ min in Figure 3*a* are attributed to natural ionospheric variation (not modeled by POLAR). Figure 3*b* illustrates the density profile one orbit after the back-away maneuver and shows this similar structure.

Let us compare the model predictions to observations for WT 1 through WT 4. The agreement is quite remarkable and affirms that the "well-behaved" wake structures associated with $T_i/T_e \approx 1$ plasmas can be adequately modeled by the physics contained in the POLAR model. There is only one significant difference between model and data. WT 2, which occurs at ≈125 m, seems to be considerably deeper than WT 4, which occurs at a little more than 100 m. *Murphy et al.* [1989] discuss this extensively, and we do not believe that, considering approximations made by the model and errors made in normalization, we could expect any better agreement. If the magnetic field, contaminant ions, and orbiter sheath do play some role, it is clear from both the model and the data that it must be a secondary one.

Studying the detail of WT 3 observations and POLAR's predicted profile, we also find good agreement. This is significant because at 45 m downstream the details of the orbiter geometry and its effect on the wake can not yet be "washed out" (the long dimension of the orbiter is ≈36 m). The agreement between model and data seems to imply that the geometric assumptions are valid and that it is permissible to use the geometric correction factor calculated from the neutral flow model, at least to first order.

Note that the center of the predicted wake seems to be

offset slightly from that observed and that the predicted density gradient seems slightly greater than observed. *Murphy et al.* [1989] discuss the accuracy with which the trajectory reconstruction takes place. This offset error is consistent with that level of precision. It is also possible that errors in normalization (constant background assumed) could produce this effect.

The difference in density gradients may be due to a slightly different plasma temperature than that modeled or may be consistent with the role played by contaminant ions in the neutralization of the space charge electric field.

Electric field data is difficult to discern from the PDP measurements because of interference from another instrument, but J. Steinberg (private communication, March 1988) has examined data from the time period of WT 3 and finds an electric field which changes sign at the wake center. This field is within a factor of 2 of that expected from a self-similar expansion. No attempt has been made to compare the predicted field computed by POLAR to the actual data, since error bars on the data are rather large. The authors may examine this as well as the RMS data [*Tribble et al.*, 1989] in more detail in a future paper. The RMS roll data may be more useful for comparison, since those data are taken at <10 m downstream, where the density depletion and electric fields are greater.

CONCLUSIONS

The sampling of PDP ion and electron densities verify that for ionospheric plasma conditions ($T_i \approx T_e$), the orbiter wake is relatively smooth in its structure from ≈30 m to distances of ≈250 m downstream. POLAR predicts this smooth wake structure and agrees with the observations to an accuracy of <30% (Table 1). For large and complex systems such as the orbiter, outgassed products may play a significant role in the structure of its wake at distances less than the characteristic body dimension. Adequate modeling in this regime requires input that details the outgassed species and rates, chemistry describing their interaction with the ionosphere, and inclusion of magnetic field to account for the pick-up ion population in the wake.

At midwake distances the magnetic field effects, if any, would appear to be secondary to the dominant role of the electric field and thermal motion already modeled by POLAR in the wake-fill process. However, for slightly larger objects or high-inclination orbits the magnetic field may have to be considered if accurate results are required. In addition, the fundamental scientific questions associated with large-body wakes will eventually require its inclusion.

For comparisons between in situ observations and models such as POLAR to be meaningful at levels better than a few tens of percent, more than simple axial or planar profiles of density are needed. Future experiments will also require good background measurements and inclusion of vector ion velocity, electric field, and particle distribution functions.

Acknowledgements. The authors wish to express their thanks to the reviewers for their constructive comments and suggestions. This work was supported by NASA MSFC contract NAS8-38207, NASA LeRC grant NAG 3-449, and by the Air Force Geophysics Lab under contract F19628-86-C-0056.

The Editor thanks W. J. Raitt and two other referees for their assistance in evaluating this paper.

REFERENCES

Chan, C., N. Hershkowitz, A. Ferreira, T. Intrator, B. Nelson, and K. Lonngren, Experimental observations at self-similar plasma expansion, *Phys. Fluids*, *27*, 266, 1984.

Crow, J. E., P. J. Aver, and J. E. Allen, The expansion of a plasma into a vacuum, *J. Plasma Phys.*, *14*, 65, 1975.

Diebold, D., N. Hershkowitz, T. Intrator, and A. Bailey, Self-similar potential in the near wake, *Phys. Fluids*, *30*, 579, 1987.

Fournier, G., and D. Pigache, Wakes in collisionless plasma, *Phys. Fluids*, *18*, 1443, 1975.

Grebowsky, J. M., H. A. Taylor, Jr., M. W. Pharo III, and N. Reese, Thermal ion perturbations observed in the vicinity of the space shuttle, *Planet. Space Sci.*, *35*, 501, 1987.

Gurevich, A. V., and L. P. Pitaevskii, Non-Linear Dynamics of a Rarefied Ionized Gas, *Prog. Aerospace Sci.*, *16*, 227, 1975.

Gurevich, A. V., L. V. Partiskaya, and L. P. Pitaevskii, Self-similar motion of a rarefied plasma, *Sov. Phys. JETP* (Engl. Transl.), *22*, 449, 1966.

Gurevich, A. V., L. P. Pitaevskii, and V. V. Smirnova, Ionospheric aerodynamics, *Space Sci. Rev.*, *9*, 805, 1969.

Hester, S. D., and A. A. Sonin, A laboratory study of wakes of ionospheric satellites, *AIAA J.*, *8*, 1090, 1970.

Katz, I., D. E. Parks, and K. H. Wright, Jr., A model of the plasma wake generated by a large object, *IEEE Transl. Nucl. Sci.*, *NS-32*(6), 4092, 1985.

Kozima, H., H. Shimizu, K. Yamada, T. Mieno, K. Yamagiwa, Self-similar flow and related phenomena of plasma around obstacles, *J. Phys. Soc. Jpn.*, *57*, 1136, 1988.

Murphy, G. B., J. Pickett, N. D'Angelo, and W. S. Kurth, Measurement of plasma parameters in the vicinity of the space shuttle, *Planet. Space Sci.*, *34*, 993, 1986.

Murphy, G. B., D. L. Reasoner, A. Tribble, N. D'Angelo, J. S. Pickett, and W. S. Kirth, The plasma wake of the shuttle orbiter, *J. Geophys. Res.*, in press, 1989.

Raitt, W. J., D. E. Siskind, P. M. Banks, and P. R. Williamson, Measurements of the thermal plasma environment of the space shuttle, *Planet. Space Sci.*, *32*, 357, 1984.

Raychaudurl, S. J. Hill, H. Chang, E. Tsikis, and K. Lonngren, An experiment on the plasma expansion into a wake, *Phys. Fluids*, *29*, 289, 1986.

Samir, U., K. H. Wright, Jr., and N. H. Stone, The expansion of a plasma into a vacuum-based phenomena and processes and application to space plasma physics, *Rev. Geophys.*, *21*, 1631, 1983.

Shawhan, S. D., G. B. Murphy, and J. S. Pickett, Plasma Diagnostics Package initial assessment of the shuttle orbiter plasma environment, *J. Spacecraft Rockets*, *21*(4), 387, 1984.

Singh, N., and R. W. Schunk, Numerical calculations relevant to the initial expansion of the polar wind, *J. Geophys. Res.*, *87*, 9154, 1982.

Stone, N. H., The aerodynamics of bodies in a rarefied, ionized gas with applications to spacecraft environmental dynamics, *NASA Tech. Pap.*, *1933*, 1981.

Stone, N. H., U. Samir, K. H. Wright, Jr., D. L. Reasoner, and S. D. Shawhan, Multiple ion streams in the near vicinity of the space shuttle, *Geophys. Res. Lett.*, *10*, 1215, 1983.

Stone, N. H., K. H. Wright, Jr., U. Samir, and K. S. Hwang, On the expansion of ionospheric plasma into the near wake of the shuttle orbiter, *Geophys. Res. Lett.*, *15*, 1169, 1988.

Tribble, H. C., J. S. Pickett, N. D'Angelo, and G. B. Murphy, Plasma density, temperature and turbulence in the wake of the shuttle Orbiter, *Planet. Space Sci.*, in press, 1989.

Wright, K. H., Jr., N. H. Stone, and U. Samir, A study of plasma expansion phenomena in laboratory-generated plasma wakes: Preliminary results, *J. Plasma Phys.*, *33*, 71, 1985.

I. Katz, S-Cubed, P.O. Box 1620, La Jolla, CA 92038.
G. Murphy, Jet Propulsion Laboratory, MS 301-460, 4800 Oak Grove Drive, Pasadena, CA 91109.

(Received December 23, 1987;
revised March 20, 1989;
accepted March 22, 1989.)

To be published in the proceedings for the
Vehicle-Environment Interaction Workshop
held at The John Hopkins University Applied
Physics Laboratory, Laurel, Maryland,
February 21 through 22, 1989

SPACECRAFT CHARGING : THE SPACECRAFT AS A FLOATING PROBE

Ira Katz
S-CUBED, A Division of Maxwell Laboratories, Inc.
P. O. Box 1620
La Jolla, CA 92038

David Cooke
Air Force Geophysics Laboratory/PHK
Hanscom Air Force Base, MA 01731

Abstract

When subject to naturally occurring fluxes of electrons with tens of kilovolts of energy, spacecraft surfaces accumulate negative charge. This charging leads to potentials as high as 20,000 volts on the spacecraft. The potential achieved depends on the electron spectrum; the density and energy spectrum of the ambient ions; the solar flux; and the materials, shape, and size of the spacecraft. While the first observations of charging were made on satellites in geosynchronous orbit, charging has been observed more recently on satellites at lower altitudes in polar orbit. The physical mechanisms which cause the charging are similar in both cases. Spacecraft surface potentials rise negatively until the electron accumulation rate is diminished and the ion collection rate enhanced so that the net current to the surfaces is zero. In low polar orbit, the enhanced ion collection dominates; in geosynchronous orbit, both processes are important.

Introduction

Spacecraft in geosynchronous orbit have been observed to charge to thousands of volts. A joint program between the Air Force and NASA investigated the phenomena. The program included both theory and experiment. The largest component was P78-2, the SCATHA (Spacecraft Charging At High Altitudes) satellite which was instrumented fully to investigate magnetospheric charging. SCATHA provided unrefuteable evidence that surface charging on spacecraft can cause discharges and operational anomalies. As reported by Koons et. al.[1], on September 22, 1982 potential differences of more than 9500 volts were measured on the satellite. At the same time, 29 pulses were detected by the Transient Pulse Monitor. Seventeen of the pulses exceeded the maximum instrument level of 7.4 volts. Coincident with the discharges were three anomalies, the most severe resulted in a two minute loss of data.

The theory component of the joint Air Force - NASA program culminated with NASCAP, the NASA Charging Analyzer Program[2,3]. NASCAP successfully modeled both frame and differential charging events observed on SCATHA[4,5]. The following briefly summarizes the mechanisms controlling spacecraft charging as they have been included in NASCAP. The understanding obtained by developing NASCAP lead to the prediction in 1980 that large satellites in polar orbit would charge from several hundred to a few thousand volts[6,7]. A computer model, POLAR (Potentials Of Large spacecraft in Auroral Region)[8], was developed to investigate the physics of auroral charging more fully. The differences between auroral and geosynchronous charging are discussed below. During 1983, instruments on board the Defense Meterological Support Program satellite 7 (DMSP 7) observed charging up to 800 volts[9]. Calculations using POLAR are compared with observed DMSP charging. The observed charging is in agreement with the mechanisms theorized in 1980.

Theory

The most basic instrument used in laboratory plasma experiments is the Langmuir probe. Typically it is a small metal sphere whose potential is swept through a limited range of voltages and the current to the sphere is measured. The current is due to charged particles from the plasma impinging upon the sphere. When the sphere potential is large compared with the kinetic energy of the plasma, only electrons are collected. When the sphere potential is very negative, only ions are collected. Between these two extremes, there is a potential at which the ion current exactly balances the electron current, so that the current to the sphere is exactly zero. This potential, at which the net current is zero, is called the floating potential. Because at a given temperature electrons move so rapidly compared with ions, the floating potential is normally negative a few θ_e, the plasma electron temperature. If the wire to the probe is cut, the probe rapidly achieves the floating potential.

The physics of spacecraft charging can be understood by regarding the spacecraft as a probe in its local, ionospheric plasma. Since there is no way for a continuous current to flow, the plasma particles rapidly charge the spacecraft to a few θe. The difference between the laboratory Langmuir probe and a spacecraft immersed in a magnetospheric substorm is that the electron energies are a few volts in the laboratory and can be tens of thousands of volts in space. Laboratory floating potentials are typically negative a few volts; in space potentials as high as -19,000 volts have been observed[10].

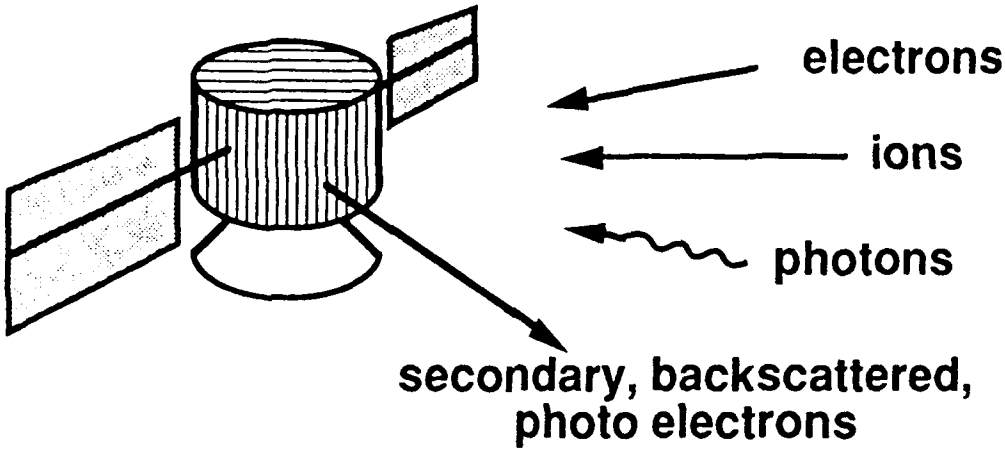

Figure 1. Highly negative potentials can result from the accumulation of charge on spacecraft surfaces.

Spacecraft are designed for purposes other than acting as plasma probes. Consequently, the interpretation and prediction of the spacecraft potential are complicated due to the complicated geometry, multiple surface materials, and the absence of an easily accessible reference ground. Each insulating spacecraft surface interacts separately with the plasma and is capacitively and resistively coupled to the frame and other surfaces. Rather than a single floating potential, there can be a different one associated with each surface. Computing surface potentials for a spacecraft is a considerably more complex problem than computing the potential on a conducting, spherical probe.

Not only is additional complexity introduced due to geometry and insulating surfaces, but currents other than incident electrons and ions must be included. Kilovolt electrons generate secondary electrons and can be backscattered from surfaces[10,11]. Kilovolt ions can also generate secondary electrons. The current density of low energy electrons generated by solar UV emission is much greater than the natural charging currents. Because of this, most spacecraft charging has been observed during eclipse, when the spacecraft is in the shadow of the earth.

For magnetospheric charging, the spacecraft is small compared with the plasma

Debye length. The electrons associated with charging typically penetrate less than a micron into the spacecraft skin. Because of this, surface coatings play a large role in determining spacecraft potentials. While the time to achieve overall current balance in very short, the order of a millisecond, the time for each surface to achieve its own equilibrium potential is thousands of times longer. The differences between the equilibrium potentials of different surfaces is referred to as differential charging.

$n_i \cong n_e \approx 10^6\ m^{-3}$

$\theta_i \approx \theta_e \approx 1 - 30\ KeV$

$\lambda_D \approx 1000\ m$

$f_p \approx 10^5\ sec^{-1}$

$j_e \approx 10^{-5}\ amps\ m^{-2}$

$j_{photo} \approx 5 \times 10^{-5}\ amps\ m^{-2}$

$electron\ stopping\ distance \approx 1 - 10 \times 10^{-7}\ m$

$\tau_{uniform\ charging} \approx 10^{-3}\ sec$

$\tau_{differential\ charging} \approx 1 - 100\ sec$

Table 1. Parameters typical of spacecraft charging in the magnetosphere.

In the plasmasphere, spacecraft usually float within a few volts of plasma potential. Upon encountering a magnetospheric substorm, the incident electron current exceeds the ion current and the vehicle charges negatively. As the potential becomes negative, the electron current diminishes because not all the electrons have the energy to overcome the potential. If the plasma were in thermal equilibrium and had a Maxwellian distribution of energies, the electron current would decrease exponentially with the negative potential. The spectrum of the electrons hitting the spacecraft would remain unchanged since the tail of a Maxwellian is still a Maxwellian.

Additional ions are attracted to the spacecraft as the potential becomes more negative. For the very low density plasma in the magnetosphere, angular momentum limits the collection of ions. The maximum impact parameter from which ions are collected is that for which the ion's collected velocity must be tangent to the spacecraft in order to conserve energy (Figure 2).

The balancing of ion and electron currents predicts a floating potential on the order of a few times the plasma temperature. Since the electron current

diminishes exponentially and the ion current increases linearly, the principle effect of the potential is to decrease the electron current.

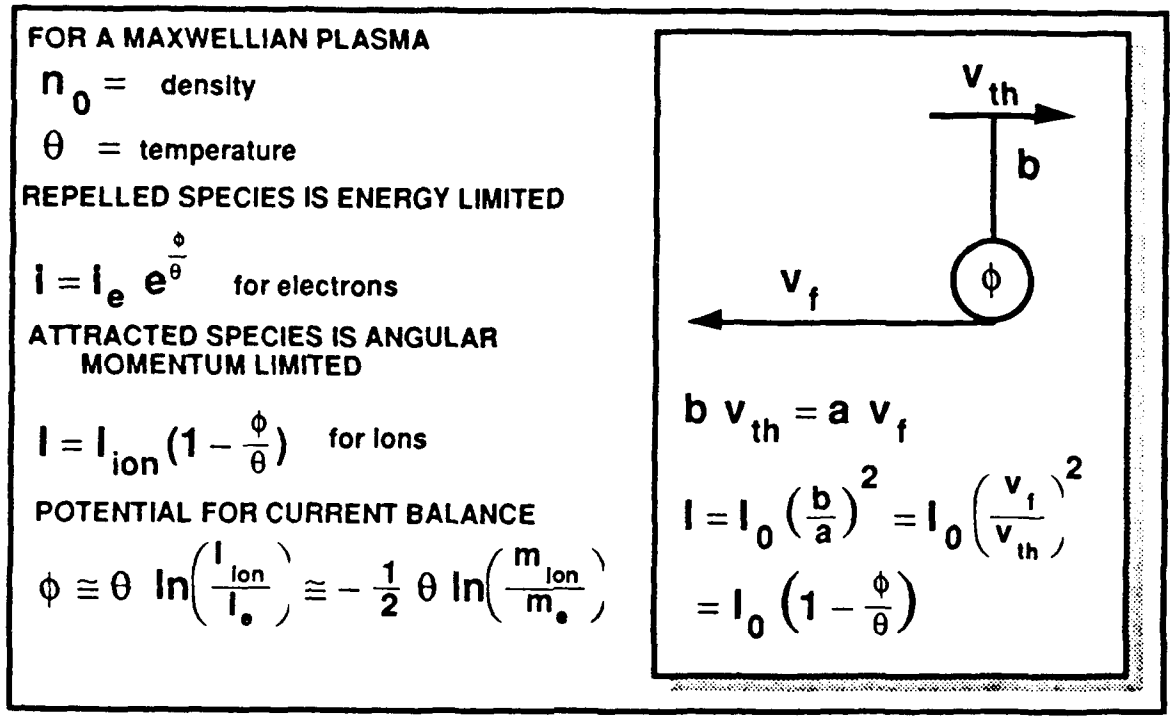

Figure 2. Orbit limited collection is based on conservation of angular momentum.

The interactions of the incident electrons and ions with the spacecraft surfaces have a profound effect on floating potentials. The most important process is secondary electron emission[11]. Because secondary electron yields are so high for many surface materials, the spacecraft floating potential is often positive! For electrons with energies between 50 eV and a few kilovolts, more than one secondary electron is emitted for every incident electron. This results in a positive charging current. Only when the electron energies exceed several thousand volts will the spacecraft charge negatively. Backscatter yields are less than unity and vary little with energy. Ion generated secondary electrons enhance the ion current and act to reduce overall charging levels.

A kapton sphere immersed in a 5 keV, 10^6 m^{-3} plasma charges to -3640 volts. The electron current which drives the charging is less than 2 X 10^{-6} A/m^2, more than half of which is immediately cancelled by secondaries and backscatter. Ion generated secondary electrons effectively triple the incident ion current. Equilibrium occurs at a potential less than the plasma temperature. Because of the secondaries and backscatter, current balance is effected equally by diminishing the electron and increasing the ions currents. Because the incident electron spectrum remains Maxwellian, electron generated secondaries and backscattered electrons remain a constant fraction of the incident current as

the spacecraft charges. The ion generated secondaries increase compared with the incident ion current because the energy of the ions increases as the spacecraft potential becomes more negative. Ion generated secondary electron yields peak for ion energies of several tens of kilovolts.

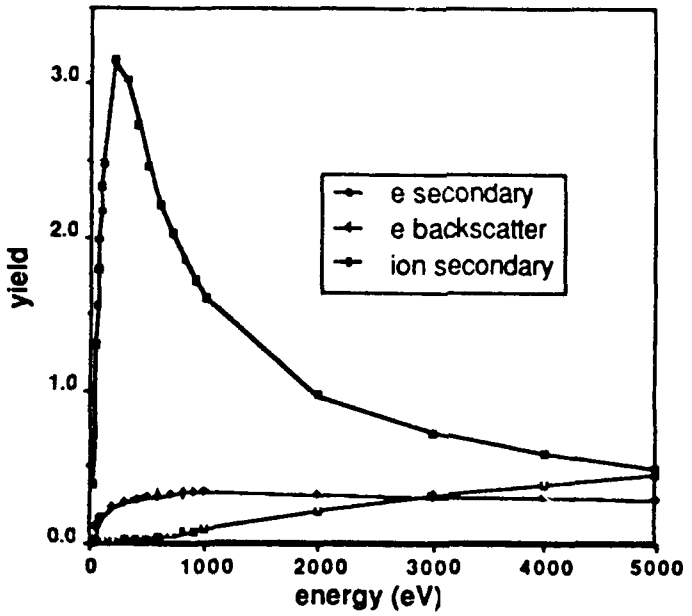

Figure 3. Electron generated secondary electron, backscatter and proton generated secondary electron yields for kapton.

Photoelectron current densities are about 10^{-4} A/m^2, typically an order of magnitude greater than incident electron currents, even before secondaries are taken into account. As a result, in sunlight high negative potentials are rarely observed on spacecraft. Charging in sunlight occurs when the low energy photoelectrons can't escape from the spacecraft because of potential barriers[12,13]. In an intense substorm, spacecraft surfaces shadowed from the sun slowly charge to thousands of volts negative, while the sunlit surfaces remain a few volts positive. After some time, a saddle point in the potential develops in front of the sunlit surfaces. Because the saddle point is driven by the photoelectron kinetic energy, it's height can never exceed a few volts. All the surfaces then charge negative at a rate corresponding with differential charging, typically a few hundred volts per minute. Sunlight charging is a multi dimensional effect calculable only by models, such as NASCAP and POLAR, which solve Poisson's equation in three dimensions[14].

Auroral Charging

The model for enhanced collection described above is generally referred to as orbit limited current collection. It is appropriate when the potential has a range larger than the largest impact parameter and is sufficiently well behaved so that no angular momentum barriers exist. Potentials that vary more slowly than with

the inverse of the radius squared satisfy these conditions. At geosynchronous orbit, the plasma is so thin that little shielding occurs and the spacecraft potential drops roughly as the inverse of the radius.

Orbit limited collection is not valid at lower altitudes, where the plasma is much denser. If the spacecraft were to charge negative, the additional ions collected would shield and thus limit the range of the potential. When the collection radius is limited by shielding due to the charge of the collected species, space charge limited collection is the appropriate theory. To model spacecraft charging in ionospheric plasma with densities greater than about 10^9 m^{-3}, space charge limited collection models must be used.

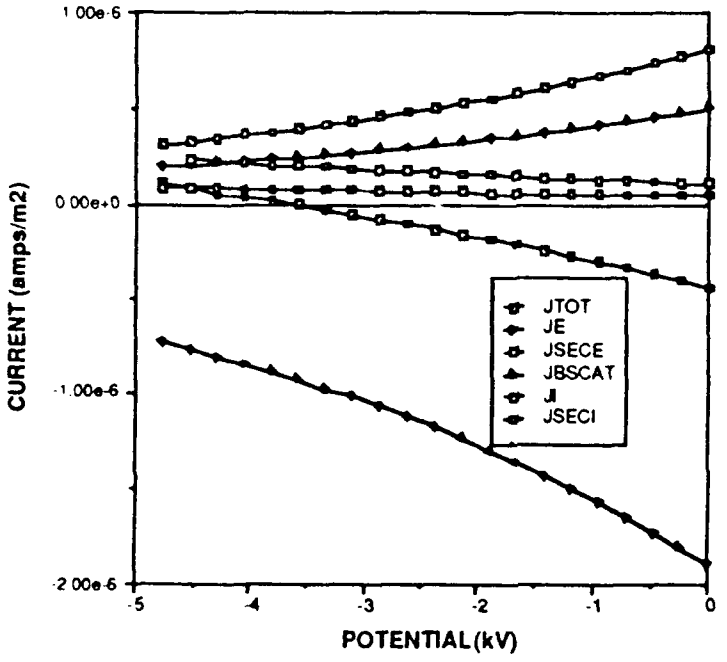

Figure 4. Current vs voltage for a kapton sphere in a 5 keV, 10^6 m^{-3} Maxwellian plasma. The floating potential is -3640 volts.

The energetic electrons which charge spacecraft in low polar orbit are the same that generate the aurora borealis. While of similar origin to substorm electrons in the magnetosphere, the auroral electron fluxes can be as much as a hundred times as intense. Some of the enhanced intensity comes from the convergence of the magnetic field lines as they approach the poles. Measured fluxes can be fit well using the analytical form suggested by Fontheim et. al.[15].

Charging of large objects in polar orbit is determined by the balance of the net auroral flux and the space charge limited ion flux. That much higher spacecraft potentials are obtained due to space charge limiting was first predicted in 1980[6]. A comparison between the potentials obtained ignoring space charge with that including it shows more than an order of magnitude difference. The

space charge limited result agrees with observation.

Spacecraft Charging Computer Codes

The NASA Charging Analyzer Program (NASCAP), was the first three dimensional spacecraft-environment interaction code. NASCAP solves Poisson's equation for spacecraft potentials due to the accumulation of charge from the magnetospheric plasma. Asymmetries are introduced by potential differences between various spacecraft surfaces due to differences in material response and solar illumination. The surface potential variations create saddle point barriers which control low energy secondary currents. NASCAP represents the spacecraft using a restricted constructive geometry technique with building blocks of cubes and segments of cubes. Because the potentials vary on a short distance scale near the spacecraft and more slowly far away, NASCAP zones the space exterior to the satellite using a sequence of nested finite element grids. The NASCAP code was first used to model the SCATHA satellite. Since then, NASCAP has been used throughout the world for spacecraft charging analysis of geosynchronous satellites.

The Air Force Geophysics Laboratory developed POLAR code models the charging of large, polar orbiting spacecraft. POLAR also calculates the plasma wake as part of the charging analysis. POLAR zones space using a staggered grid so that most of the computational space is aligned along the flow direction. The steady state sheath structure is determined by iterating between Poisson's equation for potentials and particle tracking for space charge density. The POLAR wake model has been compared with in situ measurements of the wake created by the Space Shuttle Orbiter[16].

Calculations of auroral electron induced charging of one of the Defense Meterological Support Program (DMSP) satellites have recently been compared with measurement. With the assistance of M. S. Gussenhoven, one of the observed charging electron spectra from December 1983 was fit to the Fontheim form for use in POLAR. The POLAR calculation resulted in a spacecraft potential of -230 volts, in close agreement with the observed potential of -215 volts. The differences are smaller than the possible sources of error in such a calculation. The incident electron spectrum is measured using just a few bins, the spacecraft surface properties change with time in orbit, the details of the ionic composition are not known that accurately. In general, differences larger than the 10% shown in this particular case are to be expected between calculations and observations.

Conclusion

Spacecraft charging is important because it has been shown to cause operational upsets on satellites. While of limited importance for small satellites in low polar orbit, recent data confirms predictions that charging will become more important as the size of polar orbiting spacecraft increase.

REFERENCES

1. Koons, H. C., P. F. Mizera, J. L. Roeder and J. F. Fennell, "Severe Spacecraft-Charging Event on SCATHA in September 1982," *J. Spacecraft, 25*, 239 (1988).

2. Katz, I., D. E. Parks, M. J. Mandell, J. M. Harvey, S. S. Wang and J. C. Roche, "NASCAP, A Three-Dimensional Charging Analyzer Program for Complex Spacecraft," *IEEE Transactions on Nuclear Science, NS-24(6)*, 2,276 (1977).

3. Rubin, A. G., I. Katz, M. J. Mandell, G. W. Schnuelle, P. G. Steen. D. E. Parks, J. J. Cassidy and J. C. Roche, "A Three-Dimensional Spacecraft Charging Computer Code," Edited by H. B. Garrett and C. P. Pike,*Space Systems and Their Interaction with Earth's Space Environment*, New York, AIAA (1980).

4. Katz, I., P. G. Stannard, L. Gedeon, J. C. Roche, A. G. Rubin and M. F. Tautz, "NASCAP Simulations of Spacecraft Charging of the SCATHA Satellite," Proceedings of 17th ESLAB Symposium, Noordwijk, The Netherlands, ESA SP-198, 109 (1983).

5. Schnuelle, G. W., D. E. Parks, I. Katz, M. J. Mandell, P. G. Steen, J. J. Cassidy and A. G. Rubin, "Charging Analysis of the SCATHA Satellite, " *Spacecraft Charging Technology-1978*, Edited by R. C. Finke and C. P. Pike, NASA CP-2071, AFGL-TR-79-0082 (1979). ADA084626

6. Parks, D. E. and I. Katz, "Charging of a Large Object in Low Polar Earth Orbit," *Spacecraft Charging Technology-1980*, Edited by N. J. Stevens and C. P. Pike, NASA CP-2182, AFGL TR-81-0270, 379 (1981). ADA114426

7. Katz, I. and D. E. Parks, "Space Shuttle Orbiter Charging," *J. Spacecraft, 20(1)*, 22 (1983).

8. Cooke, D. L., I. Katz, M. J. Mandell and J. R. Lilley, Jr., "A Three-Dimensional Calculation of Shuttle Charging in Polar Orbit," *Spacecraft Environment Interactions Technology-1983*, AFGL-TR-85-0018, NASA CP-2359, 205 (1985). ADA202020

9. Gussenhoven, M. S., D. A. Hardy, F. Rich, W. J. Burke and H.-C. Yeh, "High-Level Spacecraft Charging in the Low Altitude Polar Auroral Environment."

10. Whipple, E. C., "Potentials of Surfaces in Space," *Rep. Prog. Phys., 44*, 1,197 (1981).

11. Katz, I., M. J. Mandell, G. A. Jongeward and M. S. Gussenhoven, "The

Importance of Accurate Secondary Electron Yields in Modeling Spacecraft Charging," *J. Geophys. Res.*, *91*, 13,739 (986).

12. U. Fahlsen, "Plasma-Vehicle Interactions in Space--Some Aspects on Present Knowledge and Future Development," Edited by R. J. L. Grard, *Photon and Particle Interactions with Surfaces in Space*, Dordrecht-Holland (1973).

13. Mandell, M. J., I. Katz, G. W. Schnuelle, P. G. Steen and J. C. Roche, "The Decrease in Effective Photocurrents Due to Saddle Points in Electrostatic Potentials Near Differentially Charged Spacecraft," *IEEE Transactions on Nuclear Science, NS-25(6)*, 1,313 (1978).

14. Katz, I. and M. J. Mandell, "Differential Charging of High-Voltage Spacecraft: The Equilibrium Potential of Insulated Surface," *J. Geophys. Res.*, *87*, 4,533 (1982).

15. Fontheim, E. G., K. Stasiewicz, M. O. Chandler, R. S. B. Ong, E. Gombosi and R. A. Hoffman, "Statistical Study of Precipitating Electrons," *J. Geophys. Res.*, *87*, A5 (1982).

16. Murphy, G. and I. Katz, "The Polar Code Wake Model: Comparison with In-Situ Observations," J. *Geophys. Res.*, *94*, 9,065 (1989).

To be submitted for publication
in Journal of Geophysical Research

Computer Modeling of Current Collection by the Charge-2 Mother Payload

M. J. Mandell, J. R. Lilley, Jr. and I. Katz
S-CUBED Division of Maxwell Laboratories

T. Neubert
Stanford University

Neil B. Myers
Utah State University

ABSTRACT

The three-dimensional computer codes NASCAP/LEO and POLAR have been used to calculate current collection by the mother payload of the Charge-2 rocket under conditions of positive and negative potential up to several hundred volts. For negative bias (ion collection) the calculations fall about twenty-five percent above the data, indicating that the ions were less dense, colder, or heavier than the input parameters. For positive bias (electron collection) NASCAP/LEO and POLAR calculations show similar agreement with the measurements at the highest altitudes. This indicates that the current is classically magnetically limited, even during electron beam emission. However, the calculated values fall well below the data at lower altitudes. We suggest that beam-plasma-neutral interactions are responsible for the high values of collected current at altitudes below 240 kilometers.

1. Introduction

For many years electron beams have been operated from spacecraft and rockets to study long distance transport of electrons along the earth's magnetic field (Winckler, 1980). These studies were often compromised by charging of the spacecraft and/or severe perturbation of its environment as a result of beam operations. The study of these interactions has proved to be a complex and interesting field in itself.

To analyze a beam charging event, one first asks whether the observations can be explained by simple, first-order, passive current collection. This turns out to be a difficult question, since for the relevant conditions (intermediate thickness sheath with magnetic field) analytic theories exist only for spherical spacecraft. In this paper we describe the application of the three-dimensional computer codes NASCAP/LEO and POLAR to calculate charge collection by the highly cylindrical mother vehicle of the Charge-2 rocket. Calculations and measurements for negative bias (ion collection) have been reported elsewhere (Neubert *et al.*, 1989), and will only be briefly summarized here. The measurements for positive bias have also been reported previously (Myers *et al.*, 1989). In that paper the difficulty of assessing the results using theories which apply only to spheres and infinite cylinders is made apparent. The contribution of this paper is the interpretation of the positive bias results through the use of codes which correctly account for the true three-dimensional geometry of this problem.

1.1. The Charge-2 Rocket

The Charge-2 payload was launched on a Black Brant VB from White Sands Missile Range in New Mexico in December 1985. The payload consisted of mother and daughter sections which were electrically connected by an insulated tether. The mother payload was a cylinder of diameter 0.44 m and length 3.26 m; the 0.41 m nose section was coned down to a diameter of 0.33 m; the total exposed area was 4.68 m^2. The daughter payload was a cylinder of diameter 0.44 m and length 1.62 m.

Negative mother potentials were achieved by applying a potential between the mother chassis and the tether end. The daughter potential required to collect enough electrons to balance the ion current to the mother is negligible, so that the mother potential is equal to the applied potential. To maintain a steady state, the ion current collected by the mother vehicle must be equal to the tether current, which is easily measured.

Positive mother potentials were achieved by means of electron beam operations. The electron current collected by the mother is then equal to the beam current less the tether current.

The mother payload also contained an array of four "PLP" probes located on a boom at locations 25, 50, 75, and 100 cm from the rocket surface. The intent was to use these to measure the sheath profile. The 10^8 Ω probe impedance was far too low to do this in the negative bias case, but should have worked well for positive bias where the current levels are higher. The rocket potential under positive bias conditions was

inferred from the PLP probes.

1.2. The NASCAP/LEO Computer Code

NASCAP/LEO (Mandell *et al.*, 1982) is a computer code developed by the S-CUBED Division of Maxwell Laboratories under contract to NASA/Lewis Research Center to model the electrostatic interactions of a high voltage spacecraft with a plasma under conditions commonly encountered in low earth orbit. Because NASCAP/LEO is fully three-dimensional, it is able not only to treat the actual spacecraft shape, but also to account for asymmetries introduced by spacecraft motion and magnetic field effects.

NASCAP/LEO accepts as a geometrical specification a finite element surface model produced by any of several standard CAD programs. This model is then embedded in a cubic grid. Within this "primary grid", locally enhanced resolution near small but important spacecraft features may be achieved through the use of cell subdivision. To include a large volume of space about the spacecraft, the primary grid may be nested within successive "outer grids". Each outer grid has the same number of grid points as the next inner grid, but twice the physical spacing between the grid points, so that it includes eight times the volume.

NASCAP/LEO calculates electrostatic potentials in the plasma surrounding a spacecraft by using finite element and conjugate gradient methods to solve the variational form of Poisson's equation. The space charge appearing in Poisson's equation is represented as an analytic function of the plasma density and temperature and the local potential and electric field. This function reduces to linear screening at low potentials, and takes account of particle acceleration and convergence effects at high potentials. (NASCAP/LEO does not account for modification of space charge and potential structure due to magnetic fields.) Boundary conditions at object surfaces may be either specified potential or specified electric field.

Currents to spacecraft are calculated using the "sharp sheath edge" approximation. A specified electrostatic potential contour is designated as the sheath surface. Macroparticles are generated to represent the plasma thermal current (modified by spacecraft motion effects) passing through elements of area of the sheath surface. Each macroparticle is then tracked (in the calculated electric fields and specified magnetic field) until it impinges on the spacecraft or some other termination condition (e.g., escaping the grid) occurs. Thus the total current to the spacecraft and the current distribution over the spacecraft surface is determined.

NASCAP/LEO also contains surface charging algorithms, solar array models, and hydrodynamic ion models which are not relevant to the subject of this paper.

1.3. The POLAR Computer Code

POLAR (Cooke *et al.*, 1985) is a computer code developed by the S-CUBED Division of Maxwell Laboratories under contract to Air Force Geophysics Laboratory to model charging of a large spacecraft in the polar auroral environment. Thus POLAR has an environment model capable of representing the energetic and anisotropic particle fluxes observed in polar regions. However, the POLAR calculation strategy for this work did not take advantage of the sophisticated environment model. Rather, POLAR was used to calculate the current collected by the spacecraft in a fully self-consistent space charge field, to augment the NASCAP/LEO results which ignore magnetic field effects on space charge.

POLAR requires that spacecraft be modeled in a restricted geometry set similar to that used in the NASCAP/GEO code. This allows fully three-dimensional modeling for spacecraft models of modest complexity.

The POLAR grid structure was designed to encompass the wake region behind a spacecraft. Thus, the cubic grid is made up of a sequence of "bread slices" aligned approximately normal to the spacecraft velocity. Because the spacecraft velocity may not coincide with a coordinate direction, the "bread slices" may be staggered in order to be centered about the spacecraft wake. With this structure, POLAR has neither subdivided grids nor outer grids, but maintains constant resolution throughout the computational space. Since there is no loss of resolution at the sheath surface, the calculated current to a spacecraft has less dependence on the choice of sheath boundary potential than is the case with NASCAP/LEO.

The most important POLAR capability for the present purpose is its ability to use particle tracking results to modify the space charge calculated by analytic approximations. Thus, starting from a potential solution based on analytic space charge as in NASCAP/LEO, POLAR can take account of the modification of particle trajectories by magnetic fields to calculate self-consistent space charge and potential distributions.

2. Calculations for Negative Bias

Comparison of NASCAP/LEO results to the measured current collected by the Charge-2 mother payload under negative bias conditions has been published elsewhere (Neubert *et al.*, 1989). In addition to calculating the total current to the rocket, NASCAP/LEO did a fairly good job on the more difficult problem of calculating the bias on the PLP probes operating in their "floating" mode. Figure 1 shows the NASCAP/LEO model of Charge-2 in the grid, with enhanced resolution in the neighborhood of the PLP booms.

Here we will take a somewhat different point of view. By forcing NASCAP/LEO to calculate the correct current for an equivalent spherical model (Langmuir and Blodgett, 1924), we can have confidence that the difference in calculated current between the sphere and Charge-2 is due to the effects of non-spherical geometry and spacecraft

motion and not from poor resolution at the sheath boundary. The calculated results will be compared with the measurements as well. All calculations in this section are done with the plasma parameters and computational parameters shown in Table 1.

Table 1: Plasma and Computational Parameters

Plasma Density	8×10^{10} m^{-3}
Plasma Temperature	0.05 eV
Debye Length	0.588 cm.
Electron Thermal Current	4.8×10^{-4} $A\text{-}m^{-2}$
Ion [O^+] Thermal Current	2.8×10^{-6} $A\text{-}m^{-2}$
Magnetic Field	0
Spacecraft Velocity	0 ; 580 $m\text{-}sec^{-1}$
Primary Grid Resolution	10.8 cm.
Sheath Boundary Potential	(varies)
Charge-2 Model Area	4.63 m^2
Sphere Model Area	4.45 m^2

The major source of uncertainty in NASCAP/LEO current calculations lies in the choice of sheath boundary potential. In the common case that the plasma temperature is very low and many Debye lengths are contained in a computational zone, the optimal sheath boundary potential will be well above the plasma temperature. The reason for this follows from the theory of space charge limited current flow. For a plasma of density n [m^{-3}] and temperature θ [eV] the potential a distance Δx in from the physical sheath will be

$$\phi(\Delta x) = 5.1\times10^{-6}\,[(\Delta x)^4\,\theta\,n^2]^{1/3}\,.$$

For the parameters in Table 1, this value is 1.8 volts in the primary grid, 4.5 volts in the first outer grid, and 11.4 volts in the second outer grid. However, NASCAP/LEO allows at most an order-of magnitude potential drop per zone due to space charge effects. Thus, a minimum appropriate choice for the sheath boundary potential is one order-of-magnitude below $\phi(\Delta x)$, which is certainly well above the plasma temperature of .05 volts. Experience has shown that a poor choice of sheath boundary potential can lead to errors of as large as thirty percent in the calculation of collected current.

In this work we have taken care to minimize the uncertainty in the choice of sheath boundary potential. We have determined the sheath boundary potential required to obtain the correct (Langmuir and Blodgett, 1924) current to a stationary sphere of area similar to the Charge-2 model with the same plasma and computational conditions, and used that sheath boundary potential to calculate the current to the Charge-2 model. The sheath boundary potential values used ranged from 1.0 volts for the -10 volt cases to 3.4

volts for the -400 volt cases. By this procedure, we believe the computational error associated with choice of sheath boundary potential has been reduced to a few percent at most.

Table 2 shows the exact current to a sphere of area 4.45 m^2 and the calculated currents to the Charge-2 model, using the same sheath boundary potential and taking account of the spacecraft velocity of 580 m-sec^{-1}. The effect of spacecraft motion is to increase the current by ~ 40 percent at low potential, dropping to ~ 15 percent at high potential. We have also enhanced the collected current at -400 volts by fifty percent of the calculated incident ion current to account for secondary electron generation by O^+ impact. This process has a threshold at about 200 eV, and a yield of about one-half at 400 eV (Dietz and Sheffield, 1975).

Table 2. Calculated Currents [μA]
to NASCAP/LEO Sphere and Charge-2 Models

Potential	Sphere Model v = 0	Charge-2 Model v = 580 m-sec^{-1}
-10	28.9	52
-20	38.8	68
-50	62.2	98
-100	94	140
-200	148	203
-400	239	457[a]

a. Includes fifty percent enhancement due to secondary electron emission.

On figure 2 the calculations fall above the data by about twenty-five percent. Part of the discrepancy is due to the presence of a substantial NO^+ component in the ion population (Wahl, 1988; Rawer and Bradley, 1987), which lowers the ion thermal current; a 25 percent NO^+ component would reduce the collected current by about ten percent. The remaining discrepancy must be attributed to errors in the ion density value used in the calculation or to other physical uncertainties. Note that Neubert *et al.* (1989) used an ion density of 4×10^{10} m^{-3} and a temperature of 0.1 eV for all calculations.

3. Calculations for Positive Bias

In the case of positive bias (electron collection) the earth's magnetic field plays a dominant role in limiting the current collected by a spacecraft. Parker and Murphy (1967) showed, using conservation of energy and angular momentum, that a bound on the current collected by a sphere (actually, by a surface of revolution about an axis parallel to the magnetic field) is given by

$$I < 2\pi a^2 [\, 1 + (8e\phi/m\omega^2a^2)^{1/2} \,]$$

where a is the sphere radius and ω is the electron gyrofrequency, eB/m. As the Charge-2 cylinder axis was normal to the magnetic field, angular momentum is not conserved so that the Parker-Murphy bound does not strictly apply. The bound will also not apply in the presence of ionization, turbulence, or other collisional effects. Nonetheless, it is a useful guide to whether the earth's magnetic field is the dominant current limiting mechanism.

Table 3a gives the environmental parameters and spacecraft potential for the previously published (Myers *et al.*, 1989) current measurements, and Table 3b gives the measured and calculated currents. In all cases, the magnetic field was taken to be 0.4 gauss, the plasma temperature 0.052 eV, and the NASCAP/LEO sheath boundary potential 3.8 volts (chosen to give the correct sheath-limited current to the equivalent sphere in the 260 km environment). The current collected by the spacecraft is magnetically limited, as most of the electrons entering the sheath cannot cross enough field lines to be collected.

For the four data points above 240 kilometers, the measured and calculated currents are in excellent agreement. Note that both exceed the Parker-Murphy bound, indicating the difficulty of applying a symmetry-requiring theory to a non-symmetric object. (We would expect a similar, though smaller, effect in calculating magnetically limited current to the daughter rocket, so that the daughter current under positive bias, shown in Myers *et al.* (1989) as lying on the Parker-Murphy bound for the equivalent sphere, is actually slightly below the correct magnetically limited current.) These data confirm the role of the magnetic field in limiting the collected current, as the measurements fall far below the sheath-limited current (i.e., current limited only by space charge effects). The calculation of magnetically limited current is fairly insensitive to the choice of sheath boundary potential; it increases slightly with the sheath boundary potential.

Table 3a. Environments for Electron Current Data

Altitude [km]	Potential [volts]	Neutral Density[a] [10^{15} m^{-3}]	Plasma Density [10^{10} m^{-3}]
165	390	36	0.46
168	150	32	0.48
232	475	6	5.6
251a	560	3.9	8.0
251b	440	3.9	8.5
256	440	3.5	9.0
260	440	3.3	9.3

Table 3b. Calculated and Measured Collected Current [mA]

Altitude [km]	Parker-Murphy[b]	Measured	NASCAP/LEO Collected Current	NASCAP/LEO Sheath Current	POLAR Self-Consistent
165	0.4	35.8	0.6	8.3	-
168	0.3	6	0.5	3.5	-
232	5.5	20.4	7.9	42	-
251a	8.5	12.2	13.0	60	-
251b	8.1	14	12.9	52	-
256	8.6	15.6	13.5	54	-
260	8.9	18	14.1	55	22

a. MSIS-86.

b. Calculated for sphere of radius 0.6 meters.

A POLAR code calculation was done for the highest altitude measurement. POLAR, after performing a calculation similar to NASCAP/LEO, used particle trajectory information to obtain space charge densities and electrostatic potentials consistent with the trajectories in the presence of magnetic field. The POLAR model of Charge-2 was a right octagonal cylinder with length 3.3 meters and area 4.85 m^2, and the code resolution was 0.14333 meters. The higher, self-consistent space charge densities brought the sheath surface closer to the object surface, resulting in a fifty percent increase in current over the non-self-consistent calculation. We expect that the percentage change will be less for lower ambient plasma densities. This self-consistency effect explains why the measured current is consistently above the NASCAP/LEO calculated current. It is worth noting that the POLAR calculated current of 22 mA does fall below the Parker-Murphy bound (30 mA) for a sphere with diameter equal to the rocket length.

The three data points below 240 kilometers clearly show measured currents exceeding the magnetically limited value. At 232 kilometers, the collected current is about double that calculated, but well under the sheath-limited current; at 165 and 168 kilometers the measurement is one to two orders of magnitude above the calculation. Simple

ionization models are unable to predict any substantial effect within the sheath. We are forced to conclude that a complex beam-plasma interaction is taking place at these lower altitudes.

4. Conclusions

Through the use of three-dimensional modeling we are able to make unambiguous comparison with measurements, in contrast to with theories valid only for symmetric geometry.

It has been published previously that NASCAP/LEO is able to obtain excellent agreement between calculated and measured currents under conditions of negative bias. The effects of non-spherical geometry and of spacecraft motion can be separated. Also, NASCAP/LEO was able to obtain good values for the biases on the PLP probes.

Because NASCAP/LEO has poor resolution at the sheath surface, an intelligent choice of sheath boundary potential is necessary to obtain accurate current collection values. A non-optimal sheath boundary potential will lead to errors of a few tens of percent. By comparison with analytic models in the same computational environment we obtained computational results with probable accuracy of better than ten percent. By comparing the computational results for nominal ion parameters with the measurements, we conclude that errors are due to the presence of an NO^+ ion component and probably a lower ion density than the reported value. The onset of secondary electron emission above 200 eV must be taken into account.

Under positively biased (by electron beam) conditions, NASCAP/LEO calculations of magnetically limited current are in good agreement with previously published experimental results at altitudes over 240 kilometers. As the measured currents exceed the spherical Parker-Murphy bound, it was not clear before these calculations whether simple magnetically limited collection is adequate to account for the measured currents. These calculations demonstrate unambiguously that magnetically limited collection was observed above 240 kilometers. Other mechanisms are needed to explain the observations at lower altitudes.

As NASCAP/LEO does not treat the modification of space charge by magnetic field effects, we have run the POLAR code to study the effect of fully self-consistent space charge on the highest altitude measurement. For this case, fully self-consistent space charge led to an increase in current of about fifty percent, bringing the calculation into better agreement with the measurement, and explaining the general trend that the non-self-consistent calculations lie below the high altitude measurements. As the plasma density decreases and the sheath lies farther beyond the Parker-Murphy radius, we expect the difference in space charge treatments to have less effect on the calculated currents. Note also that the fully self-consistent result is about twenty percent high relative to the measurement; this is a comparable error to the negative bias results, again suggesting that the actual densities were below the nominal values.

In summary, the calculations clearly demonstrate that the published current collection data above 240 kilometers can be understood in terms of simple, quasi-static sheath processes with magnetic limiting for electrons. The three low altitude electron current measurements lie well above the predictions of such theories and indicate that more complex physical mechanisms are at work.

References

Cooke, D. L. *et al.*, "A three-dimensional calculation of shuttle charging in polar orbit", *Spacecraft Environmental Interactions Technology-1983,* NASA CP-2359, AFGL-TR-85-0018, 205-228, 1985. ADA202020

Dietz, L. A. and J. C. Sheffield, "Secondary electron emission induced by 5-30-kev monatomic ions striking thin oxide films", *J. Appl. Phys. 46,* 4361-4370, 1975.

Langmuir, I. and K. B. Blodgett, "Current limited by space charge flow between concentric spheres", *Phys. Rev. 24,* 49-59, 1924.

Mandell, M. J., I. Katz and D. L. Cooke, "Potentials on large spacecraft in LEO", *IEEE Trans. Nucl. Sci. NS-29,* 1584-1588, 1982.

Myers, N. B. *et al.*, "A comparison of current-voltage relationships of collectors in the earth's ionosphere with and without electron beam emission", *Geophys. Res. Lett. 16,* 365-368, 1989.

Neubert, T. *et al.*, "The sheath structure around a negatively charged rocket payload". To be published in *J. Geophys. Res.*, 1989.

Parker, L. W. and B. L. Murphy, "Potential buildup on an electron-emitting ionospheric satellite", *J. Geophys. Res. 72,* 1631-1636, 1967.

Rawer, K. and P. A. Bradley, *International Reference Ionosphere - Status 1986/87.* Pergamon Press.

Wahl, S., "Space Environments and Interactions Programs, Vol. 4: Ionosphere", Syscon Corporation, Montrose, CA., 1988.

Winckler, J. R., "The application of artificial electron beams to magnetospheric research", *J. Geophys. Res. 18,* 659-682, 1980.

Figure Captions

Figure 1. NASCAP/LEO gridding around the Charge-2 model, showing fine resolution about the PLP booms and halving of resolution in the outer grid.

Figure 2. Ion collection current: points and line: this paper; horizontal error bars: flight results.

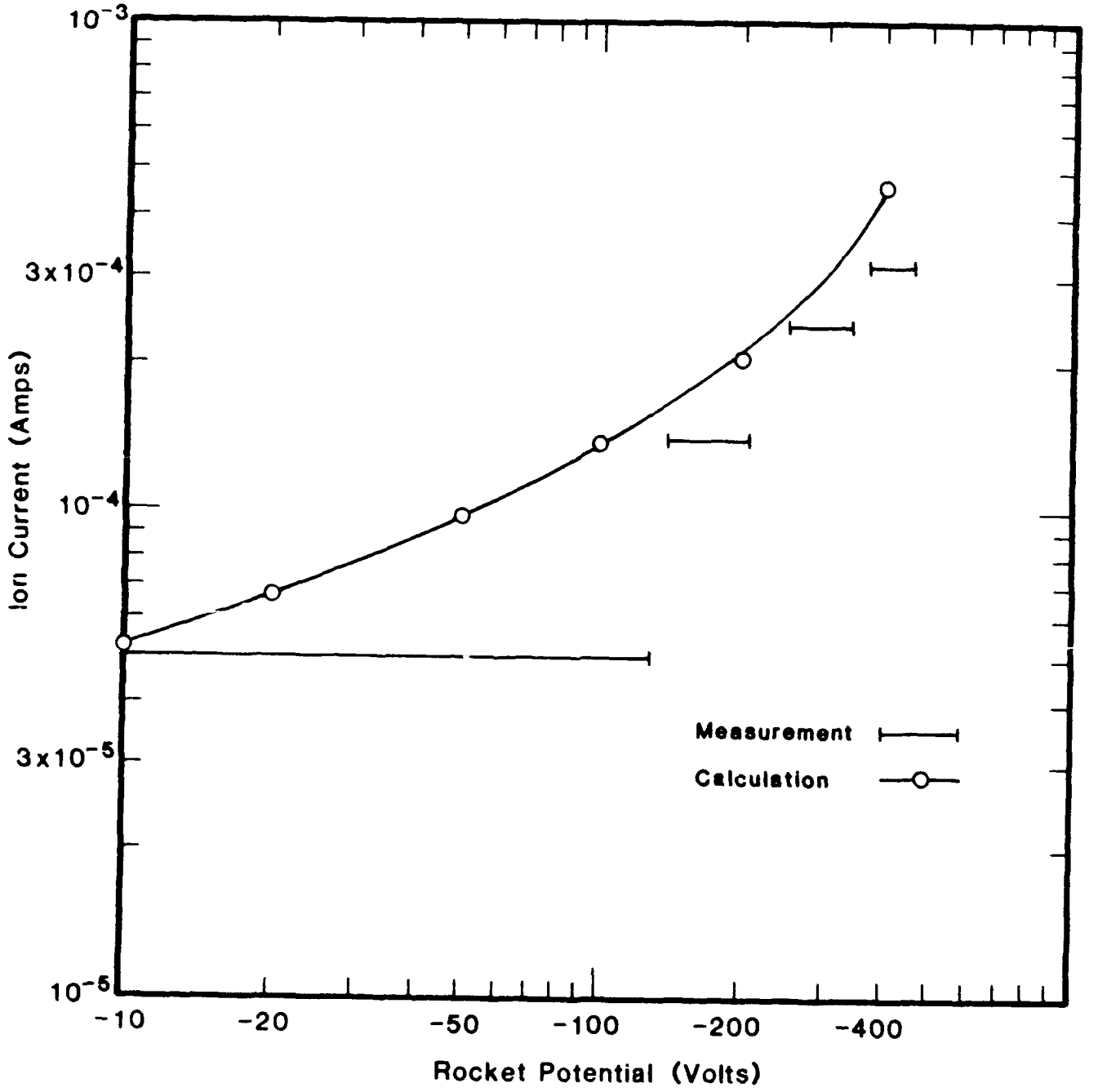
10^{-3}
$3x10^{-4}$
10^{-4}
$3x10^{-5}$
10^{-5}
Ion Current (Amps)
-10
-20
-50
-100
-200
-400
Rocket Potential (Volts)
Measurement
Calculation

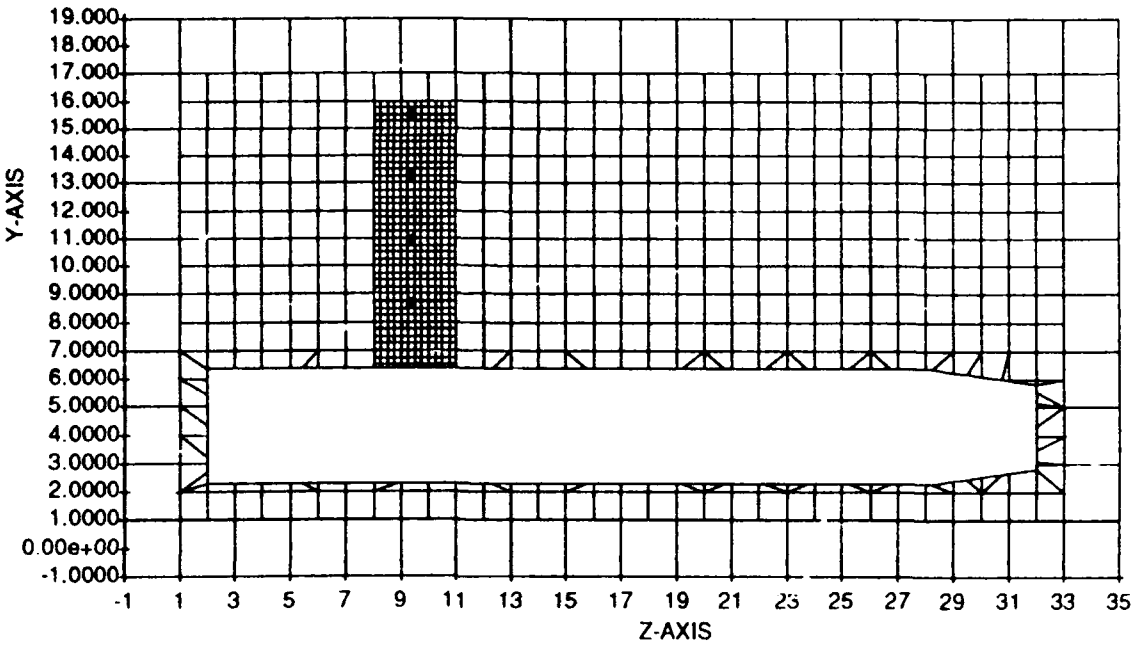

-1.00 <Z< 35.00, -1.00 <Y< 19.00, CUTPLANE OFFSET X= 9.00

REFERENCES

Chan, C., N. Hershkowitz, A. Ferreira, T. Intrator, B. Nelson, and K. Lonngren, Experimental Observations at Self-similar Plasma Expansion, *Physics of Fluids, Vol. 27*, p. 266, 1984.

Cooke, D., M. Tautz, J. Lilley, "Polar Code Simulation of DMSP Satellite Auroral Charging", Paper presented at AIAA meeting, Reno, Nevada, January 11, 1989.

Crow, J. E., P. J. Aver, and J. E. Allen, The Expansion of a Plasma into a Vacuum, *Journal of Plasma Physics, Vol. 14*, p. 65, 1975.

Gussenhoven, M. S., D. A. Hardy, F. Rich, W. J. Burke, and H. -C. Yeh, High-level Spacecraft Charging in the Low-altitude Polar Auroral Environment, *Journal of Geophysical Research, Vol. 90*, p. 11, 009, 1985.

Katz, I., D. E. Parks, and K. H. Wright, Jr., A Model of the Plasma Wake Generated by a Large Object, *IEEE Transactions on Nuclear Science, Vol. NS-32(6)*, p. 4,092, 1985.

Katz, I., G. A. Jongeward, V. A. Davis, M. J. Mandell, R. A. Kuharski, J. R. Lilley, Jr., W. J. Raitt, D. L. Cooke, R. B. Torbert, G. Larson, and D. Rau, Structure of the Bipolar Plasma Sheath Generated by SPEAR I, *Journal of Geophysical Research, Vol. 94*, p. 1,450, 1989.

Murphy, G. and Katz, I., The POLAR Code Wake Model: Comparison with in Situ Observations, *Journal of Geophysical Research, Vol. 94*, p. 9,065, 1989.

Murphy, G. B., D. L. Reasoner, A. Tribble, N. D'Angelo, J. S. Pickett, and W. S. Kurth, The Plasma Wake of the Shuttle Orbiter, *Journal of Geophysical Research, Vol. 94*, p. 6,866, 1989.

Myers, N. B., W. J. Raitt, B. E. Gilchrist, P. M. Banks, T. Neubert, P. R. Williamson, and S. Sasaki, A Comparison of Current-Voltage Relationships of Collectors in the Earth's Ionosphere with and without Electron Beam Emission, *Geophysical Research Letters, Vol. 16,* p. 365, 1989.

Parks, D.E. and Katz, I., Charging of a Large Object in Low Polar Earth Orbit, *Spacecraft Charging Technology 1980*, NASA Conference Publication 2182, AFGL-TR-81-0270, 1980. ADA114426

Parrot, M. J. M., L. R. O. Storey, L. W. Parker, and J. G. Laframboise, Theory of Cylindrical and Spherical Langmuir Probes in the Limit of Vanishing Debye Number, *Physics of Fluids, Vol. 25*, p. 2,388, 1982.

Wright, K. H., Jr., N. H. Stone, and U. Samir, A Study of Plasma Expansion Phenomena in Laboratory-generated Plasma Wakes: Preliminary Results, *Journal of Plasma Physics, Vol. 33*, p. 71, 1985.